INTERNATIONAL JOURNAL FOR NUMERICAL METHODS IN FLUIDS, VOL. 18, 127–162 (1994)

p-VERSION LEAST SQUARES FINITE ELEMENT FORMULATION FOR TWO-DIMENSIONAL, INCOMPRESSIBLE, NON-NEWTONIAN ISOTHERMAL AND NON-ISOTHERMAL FLUID FLOW

BRENT C. BELL AND KARAN S. SURANA*

The University of Kansas, Department of Mechanical Engineering, 3013 Learned Hall, Lawrence, KS 66045, U.S.A.

SUMMARY

This paper presents a p-version least squares finite element formulation (LSFEF) for two-dimensional, incompressible, non-Newtonian fluid flow under isothermal and non-isothermal conditions. The dimensionless forms of the differential equations describing the fluid motion and heat transfer are cast into a set of first-order differential equations using non-Newtonian stresses and heat fluxes as auxiliary variables. The velocities, pressure and temperature as well as the stresses and heat fluxes are interpolated using equal-order, C^0-continuous, p-version hierarchical approximation functions. The application of least squares minimization to the set of coupled first-order non-linear partial differential equations results in finding a solution vector $\{\delta\}$ which makes the partial derivatives of the error functional with respect to $\{\delta\}$ a null vector. This is accomplished by using Newton's method with a line search.

The paper presents the implementation of a power-law model for the non-Newtonian Viscosity. For the non-isothermal case the fluid properties are considered to be a function of temperature. Three numerical examples (fully developed flow between parallel plates, symmetric sudden expansion and lid-driven cavity) are presented for isothermal power-law fluid flow. The Couette shear flow problem and the 4:1 symmetric sudden expansion are used to present numerical results for non-isothermal power-law fluid flow. The numerical examples demonstrate the convergence characteristics and accuracy of the formulation.

KEY WORDS Least squares Finite element p-version Error functional Power-law-fluid Non-isothermal Degrees of freedom p-convergence Hierarchical Newton's method Line search

INTRODUCTION

The finite element method has been proven to be a powerful tool in the solution of a variety of fluid flow problems. The majority of published finite element formulations are based on either variational or weighted residual methods. Variational methods produce the 'best' approximation to the exact solution of the associated variational problem. However, the variational principle in general cannot be constructed for systems described by non-linear partial differential equations. Galerkin methods, collocation and least squares methods are possible alternatives and are special cases of the general weighted residual method. Galerkin-based formulations of the steady incompressible Navier–Stokes equations in primitive variables (P, u, v) lead to several

* Author to whom correspondence should be addressed.

0271–2091/94/020127–36$23.00

Received 16 June 1992
Revised 29 July 1993

well-known difficulties.[1] Special procedures for circumventing these difficulties have been investigated and are reported in the literature.[2–6]

The least squares finite element method has been advocated as a unified method for fluid dynamics applications[7] and satisfies the criteria desirable in variational methods.[8] The least squares finite element method has been applied to elliptic,[9] hyperbolic[10] and mixed[11] partial differential equations. Applications include boundary layer flow,[12] gas dynamics,[13] Stokes flow,[14] inviscid compressible flow,[15] convection–diffusion[16] and phase change problems.[17] p-Version-based finite element formulations provide superior convergence behaviour over h-version-based elements,[18] yet the majority of CFD finite element research has been concentrated on the use of low-order element approximations. Jiang and Sonnad[19] formulated p-version least squares finite elements for two-dimensional, incompressible fluid flow using the pressure–velocity–vorticity approach and Legendre polynomials. Winterscheidt and Surana[1,20,21] have presented p-version least squares formulations for Burgers' equation, convection–diffusion and two-dimensional, incompressible Newtonian flow. In these formulations the describing equations were cast into a series of first-order equations (by introducing auxiliary variables) for which the least squares finite element formulation was constructed using equal-order, C^0-continuous, p-version hierarchical approximation functions for both primary and auxiliary variables.

It is the purpose of this paper to develop a p-version finite element framework based on the least squares approach for the solution of problems involving non-Newtonian fluids, specifically fluids described by generalized Newtonian models. The flow of an incompressible Newtonian fluid is described by Navier–Stokes equations in which the only non-linear terms are the convection terms in the momentum equations. The viscosity of a non-Newtonian fluid is a function of the flow field parameters. As a result, an additional source of non-linearity is introduced into the system of equations describing the flow. It has been reported that for generalized Newtonian fluid models this additional non-linearity can result in lack of convergence or extremely slow convergence of the iterative solution procedure.[22–24] These investigations show the importance of the solution procedure, while other studies have concentrated on adaptive mesh refinement techniques.[25,26] The extent of additional difficulties encountered in the solution of non-Newtonian fluid flow problems may also be influenced by the particular finite element formulation.

Both Galerkin and penalty finite element formulations have been used[22,24,27] in the solution of Newtonian as well as non-Newtonian fluid flow problems. The disadvantages of these methods are that they produce non-symmetric matrices and involve problem-dependent parameters which must be carefully chosen to ensure convergence to an accurate solution. For instance, in the penalty function formulation the penalty parameter influences the extent to which continuity is satisfied and the formations based on the Galerkin approach often require the use of upwinding to suppress spurious oscillations in the computed solution.

Many published finite element solutions for fluid flow problems consider only isothermal flow conditions where the energy equation is not included in the formulation. In this case the effects of heat generation by viscous dissipation (important in highly viscous polymer flows for example) and heat exchange with flow boundaries are not taken into account. Even in the formulations of non-isothermal fluid flow problems, often the energy equation is considered to be decoupled from the continuity and momentum equations and is solved separately. However, in the general case of non-isothermal fluid flow where one or more of the fluid transport properties are dependent on temperature, the continuity, momentum and energy equations are fully coupled and must be solved simultaneously to obtain accurate solutions for the velocity, pressure and temperature fields. This represents a difficult problem considering the

non-linear character of the momentum, energy and constitutive (for non-Newtonian viscosity) equations.

In this paper the least squares formulation procedure is combined with the *p*-version finite element approximation to produce a general framework for the solution of two-dimensional, steady state, incompressible flow problems involving inelastic non-Newtonian fluids which can be described by the power-law model. Formulations for both isothermal and non-isothermal fluid flows are considered. For the non-isothermal case the energy equation is solved simultaneously with the other equations so that non-isothermal flow problems involving temperature-dependent transport properties can be solved. The use of the *p*-version element approximation in the least squares finite element method is an important aspect of the present formulation. It has been demonstrated that the *p*-version-based finite element formulations possess superior convergence characteristics to the *h*-version-based elements.[18] The present formulation, when combined with Newton's method with a line search, produces symmetric matrices even though the differential equations describing the flow are non-linear.

A summary of the formulations for both isothermal and non-isothermal non-Newtonian fluid flow is presented in the following sections. In addition, the effect of two different non-dimensional forms of the equations of fluid motion on the convergence behaviour of Newton's method is investigated. Three numerical examples are presented (fully developed flow between parallel plates, a 2:1 symmetric sudden expansion and a lid-driven cavity) to demonstrate the convergence characteristics and the accuracy of the present formulation for isothermal power-law fluids. Two numerical examples (Couette shear flow and a 4:1 symmetric sudden contraction) are given for non-isothermal flow. In both of these examples (for the non-isothermal case) power-law fluids with a temperature-dependent viscosity are considered. Our results for flow between parallel plates and Couette shear flow are compared with the analytical solutions[28,29] and serve as an accuracy check for isothermal and non-isothermal cases.

The 4:1 symmetric sudden contraction represents a difficult problem and has become a standard test problem in computational fluid dynamics for both Newtonian and non-Newtonian fluid flow. Two of the more thorough discussions of the characteristics of contraction flow were given by Boger[30,31] for an axisymmetric geometry. The majority of the published finite element solutions for this problem consider only isothermal conditions. Mitsoulis and Vlachopoulos[32] studied the effect of the Reynolds number for a 10:1 planar contraction using the Galerkin method. Reddy *et al.*[33] report results for a 4:1 contraction involving non-Newtonian fluids using the penalty finite element method. Crochet *et al.*[34] discuss both the Galerkin and penalty finite element methods for generalized Newtonian fluids and present results for the 4:1 contraction problem. Hawken *et al.*[35] used a Taylor–Galerkin fractional step method to obtain the steady state solution for incompressible flow in 2:1 and 4:1 contractions. Durst *et al.*[36] give experimental results for both 2:1 and 4:1 contractions.

Perhaps the first to apply the finite element method to the non-isothermal flow in a 4:1 contraction were Douglas and Roylance.[37] In their work the effect of viscous dissipation on the temperature field of a Newtonian fluid was studied. The Galerkin weighted residual method with upwinding (for high Peclet numbers) was used to solve the decoupled energy equation. Mitsoulis and Vlachopoulos[38] also used the Galerkin method with upwinding to study viscous dissipation in the creeping flow of Newtonian fluids with a temperature-dependent viscosity and power-law fluids without a temperature-dependent viscosity for a 10:1 contraction. Tanguy and co-workers[39,40] used an augmented Lagrangian formulation to study the non-isothermal flow of a Carreau-A fluid in a 10:1 contraction. In both of these last two

studies the energy equation was handled separately from the other equations describing the fluid motion and coupling of the energy equation was accomplished in a cyclic manner.

In this paper we present a *p*-version least squares finite element formulation for the non-isothermal flow of generalized Newtonian fluids with a temperature-dependent viscosity and thermal conductivity. The isothermal non-Newtonian fluid flow can be treated as a special case in which the energy equation is absent and thus the non-Newtonian viscosity is not a function of temperature. The non-isothermal conditions can be caused by either viscous dissipation or heat exchange with the flow boundaries or both. The Reynolds number in all numerical examples was chosen so that both convection and diffusion terms were important. As will be demonstrated, upwinding techniques and 'reduced' integration methods are not required in the present formulation to obtain accurate solutions for the velocity, pressure and temperature fields. In addition, the energy equation is solved simultaneously with the other equations.

LEAST SQUARES FINITE ELEMENT FORMULATION (GENERAL DERIVATION)

Full details of the least squares finite element formulation (LSFEF) procedure for a system of non-linear differential equations and the solution method have been presented by Winterscheidt and Surana.[1] Here we present a brief summary of the pertinent equations without derivations.

For a system of N differential equations and a discretization with NE elements the total error functional I can be written as the sum of the error functionals I^e for the elements:

$$I = \sum_{e=1}^{NE} I^e = \sum_{e=1}^{NE} \sum_{i=1}^{N} \int_{\Omega^e} (E_i^e)^2 \, d\Omega, \tag{1}$$

where E_i^e, $i = 1, 2, \ldots, N$, are the errors which result when the finite element approximation to the true solution is substituted into the differential equations. In the LSFEF we minimize the total error functional given by (1), which yields

$$\frac{\partial I}{\partial \{\delta\}} = \{g\} = \sum_{e=1}^{NE} \frac{\partial I^e}{\partial \{\delta^e\}} = \sum_{e=1}^{NE} \{g^e\} = 2 \sum_{e=1}^{NE} \sum_{i=1}^{N} \left\{ \frac{\partial E_i^e}{\partial \{\delta^e\}} \right\} E_i^e \, d\Omega = \{0\}, \tag{2}$$

where $\{\delta\}$ is the vector of nodal degrees of freedom for the entire discretization and $\{\delta^e\}$ are the nodal degrees of freedom for an element e. Thus least squares minimization leads to finding a $\{\delta\}$ which makes $\{g\}$ a null vector. Since $\{g\}$ is a non-linear function of $\{\delta\}$, we expand $\{g\}$ in a Taylor series about a starting vector $\{\delta_0\}$ and retain only linear terms in $\{\Delta\delta\}$, which yields

$$\left[\sum_{e=1}^{NE} \left[\frac{\partial \{g^e\}}{\partial \{\delta^e\}} \right]_{\{\delta_0\}} \right] \{\Delta\delta\} = \left[\sum_{e=1}^{NE} [H^e]_{\{\delta_0\}} \right] \{\Delta\delta\} = - \sum_{e=1}^{NE} \{g^e(\{\delta_0^e\})\}, \tag{3}$$

where $\{H^e\}$ is the element Hessian matrix and is given by

$$[H^e] = 2 \sum_{i=1}^{N} \int_{\Omega^e} \left[\left\{ \frac{\partial E_i^e}{\partial \{\delta^e\}} \right\} \left\{ \frac{\partial E_i^e}{\partial \{\delta^e\}} \right\}^{\mathrm{T}} + E_i^e \frac{\partial}{\partial \{\delta^e\}} \left\{ \frac{\partial E_i^e}{\partial \{\delta^e\}} \right\} \right] d\Omega. \tag{4}$$

The improved value of the solution is obtained using

$$\{\delta\} = \{\delta_0\} + \alpha\{\Delta\delta\}. \tag{5}$$

The scalar α is selected to minimize I. This procedure is referred to as Newton's method with a line search. In the present work we use $\{\delta_0\} = \{0\}$ and $\alpha = 1$ for the first iteration; the line search is used for subsequent iterations. Numerical values of $[H^e]$ are calculated without the second term in the integrand of $[H^e]$. This improves the convergence behaviour of Newton's method. Ease of programming and computational efficiency are other advantages when this term is deleted.[1] A detailed discussion of the line search and the necessary and sufficient conditions for minima of I have been given by Winterscheidt and Surana[1] and are not presented here for the sake of brevity.

In the following we present a derivation and the pertinent details of the p-version least squares finite element formulation for non-isothermal non-Newtonian fluid flow for power-law fluids where the viscosity and the thermal conductivities are temperature-dependent. Details of the formulation for the isothermal case can be obtained as a special case.

EQUATIONS OF FLUID MOTION (NON-ISOTHERMAL CASE)

The continuity, momentum, constitutive and energy equations for the steady-state, two-dimensional incompressible flow of a generalized Newtonian fluid are given by

$$\begin{aligned}
&\frac{\partial \hat{u}}{\partial \hat{x}} + \frac{\partial \hat{v}}{\partial \hat{y}} = 0,\\
&\hat{\rho}\left(\hat{u}\frac{\partial \hat{u}}{\partial \hat{x}} + \hat{v}\frac{\partial \hat{u}}{\partial \hat{y}}\right) + \frac{\partial \hat{P}}{\partial \hat{x}} - \left(\frac{\partial \hat{\tau}_{xx}}{\partial \hat{x}} + \frac{\partial \hat{\tau}_{xy}}{\partial \hat{y}}\right) = 0,\\
&\hat{\rho}\left(\hat{u}\frac{\partial \hat{v}}{\partial \hat{x}} + \hat{v}\frac{\partial \hat{v}}{\partial \hat{y}}\right) + \frac{\partial \hat{P}}{\partial \hat{y}} - \left(\frac{\partial \hat{\tau}_{xy}}{\partial \hat{x}} + \frac{\partial \hat{\tau}_{yy}}{\partial \hat{y}}\right) = 0,\\
&\hat{\tau}_{xx} - 2\hat{\eta}_v\frac{\partial \hat{u}}{\partial \hat{x}} = 0,\\
&\hat{\tau}_{xy} - \hat{\eta}_v\left(\frac{\partial \hat{u}}{\partial \hat{y}} + \frac{\partial \hat{v}}{\partial \hat{x}}\right) = 0,\\
&\hat{\tau}_{yy} = 2\hat{\eta}_v\frac{\partial \hat{v}}{\partial \hat{y}} = 0,\\
&\hat{\rho}\hat{C}_p\left(\hat{u}\frac{\partial \hat{T}}{\partial \hat{x}} + \hat{v}\frac{\partial \hat{T}}{\partial \hat{y}}\right) - \left(\frac{\partial \hat{q}_x}{\partial \hat{x}} + \frac{\partial \hat{q}_y}{\partial \hat{y}}\right) - \left[\hat{\tau}_{xx}\left(\frac{\partial \hat{u}}{\partial \hat{x}}\right) + \hat{\tau}_{xy}\left(\frac{\partial \hat{u}}{\partial \hat{y}} + \frac{\partial \hat{v}}{\partial \hat{x}}\right) + \hat{\tau}_{yy}\left(\frac{\partial \hat{v}}{\partial \hat{y}}\right)\right] = 0,\\
&\hat{q}_x - \hat{k}_{xx}\frac{\partial \hat{T}}{\partial \hat{x}} - \hat{k}_{xy}\frac{\partial \hat{T}}{\partial \hat{y}} = 0,\\
&\hat{q}_y - \hat{k}_{yy}\frac{\partial \hat{T}}{\partial \hat{y}} - \hat{k}_{xy}\frac{\partial \hat{T}}{\partial \hat{x}} = 0.
\end{aligned} \tag{6}$$

In this study the fluid density $\hat{\rho}$ and the heat capacity $\hat{C}_p$ are considered to be constant. In addition, the fluid is considered to be isotropic with a constant thermal conductivity and

hence $\hat{k}_{xy} = 0$ and $\hat{k}_{xx} = \hat{k}_{yy}$. The generalized Newtonian viscosity $\hat{\eta}_v$ depends on the local shear rate (flow field parameters) and temperature of the fluid. The subscript 'v' is used to distinguish the generalized Newtonian viscosity from the natural co-ordinate direction η discussed later.

The manner in which the constitutive equations in (6) are written is of the same general form as those for a Newtonian fluid. It is for this reason that relationships of this form are called generalized Newtonian fluid models. The specific form of $\hat{\eta}_v$ is chosen to describe the physical behaviour of the fluid of interest. The simplest is the Newtonian model where $\hat{\eta}_v$ is constant for the entire flow field. There are many non-Newtonian viscosity models which are used to describe more complicated fluid behaviour such as shear thinning, shear thickening and elasticity.[41,42] In the following we discuss the inelastic power-law model.

Of the many generalized Newtonian models, the power-law model is the most commonly used. For this reason we use it here to describe the shear rate dependence of $\hat{\eta}_v$; however, any other generalized Newtonian model could also be used, such as the Carreau–Yasuda or Bingham plastic models.[41,42] The power-law model is given by

$$\hat{\eta}_v = \hat{m}(\hat{I}_2)^{(n-1)/2}, \tag{7}$$

where $\hat{m}$ is the fluid consistency, $\hat{I}_2$ is the second invariant of the rate-of-strain tensor and n is the power-law index. For values of n between zero and unity the viscosity is shear thinning, for $n > 1$ the viscosity is shear thickening and for $n = 1$ equation (7) reduces to the Newtonian viscosity model with $\hat{m} = \hat{\mu}$.

For two-dimensional flow the explicit form of $\hat{I}_2$ is given by

$$\hat{I}_2 = 2\left(\frac{\partial \hat{u}}{\partial \hat{x}}\right)^2 + 2\left(\frac{\partial \hat{v}}{\partial \hat{y}}\right)^2 + \left(\frac{\partial \hat{u}}{\partial \hat{y}} + \frac{\partial \hat{v}}{\partial \hat{x}}\right)^2. \tag{8}$$

The temperature dependence of the viscosity is usually described by considering the temperature dependence of $\hat{m}$ and n separately. For almost all fluids the temperature dependence of n is small compared with that of $\hat{m}$[42] and will be neglected in this work. The particular choice of the relationship used to describe the temperature dependence of $\hat{m}$ is problem-dependent and will be discussed in the numerical examples section.

DIMENSIONLESS FORM OF THE EQUATIONS OF FLUID MOTION AND HEAT TRANSFER

In order to build a general framework for the solution of the equations of motion and heat transfer (6) using the p-version LSFEF, it is desirable to cast equations (6)–(8) into dimensionless form. The choice of the dimensionless form of these equations has a dramatic effect on the convergence of the iterative process used for obtaining the numerical solution (see Example 2).

Two different non-dimensional forms of equations (6)–(8) are considered. These two forms arise as a result of the choice of the characteristic scale for the stresses. If the characteristic viscous stress ($\eta_0 V_0/L$) is chosen to scale the stresses, the Reynolds number appears in the momentum equations. If the characteristic kinetic energy ($\rho_0 V_0^2$) is used to scale the stresses, the Reynolds number appears in the stress equations. As will be demonstrated later, the first choice has undesirable effects which lead to non-convergence of the iterative solution procedure or convergence to spurious solutions for a variety of problems.

In the present study we scale the stresses using the characteristic kinetic energy. The following dimensionless variables are used:

$$
\begin{aligned}
&x = \frac{\hat{x}}{L}, \qquad y = \frac{\hat{y}}{L}, \\
&\rho = \frac{\hat{\rho}}{\rho_0}, \qquad m = \frac{\hat{m}}{m_0}, \qquad C_p = \frac{\hat{C}_p}{C_{p_0}}, \qquad k = \frac{\hat{k}}{k_0}, \\
&u = \frac{\hat{u}}{V_0}, \qquad v = \frac{\hat{v}}{V_0}, \\
&P = \frac{\hat{P} - P_0}{\rho_0 V_0^2}, \qquad T = \frac{\hat{T} - T_0}{T_1 - T_0}, \\
&\tau_{xx} = \frac{\hat{\tau}_{xx}}{\tau_0}, \qquad \tau_{xy} = \frac{\hat{\tau}_{xy}}{\tau_0}, \qquad \tau_{yy} = \frac{\hat{\tau}_{yy}}{\tau_0}, \\
&q_x = \frac{\hat{q}_x}{q_0}, \qquad q_y = \frac{\hat{q}_y}{q_0},
\end{aligned} \tag{9}
$$

where $\tau_0 = \rho_0 V_0^2$ and $q_0 = k_0(T_1 - T_0)/L$.

Using these variables, equations (6) can be transformed into

$$
\begin{aligned}
&\frac{\partial u}{\partial x} + \frac{\partial v}{\partial y} = 0, \\
&u\frac{\partial u}{\partial x} + v\frac{\partial u}{\partial y} + \frac{\partial P}{\partial x} - \left(\frac{\partial \tau_{xx}}{\partial x} + \frac{\partial \tau_{xy}}{\partial y}\right) = 0, \\
&u\frac{\partial v}{\partial x} + v\frac{\partial v}{\partial y} + \frac{\partial P}{\partial y} - \left(\frac{\partial \tau_{xy}}{\partial x} + \frac{\partial \tau_{yy}}{\partial y}\right) = 0, \\
&\tau_{xx} - 2\eta_v \frac{\partial u}{\partial x} = 0, \\
&\tau_{xy} - \eta_v\left(\frac{\partial u}{\partial y} + \frac{\partial v}{\partial x}\right) = 0, \\
&\tau_{yy} - 2\eta_v \frac{\partial v}{\partial y} = 0, \\
&\left(u\frac{\partial T}{\partial x} + v\frac{\partial T}{\partial y}\right) - \frac{1}{Re_n Pr_n}\left(\frac{\partial q_x}{\partial x} + \frac{\partial q_y}{\partial y}\right) - \frac{Br_n}{Pr_n}\left[\tau_{xx}\left(\frac{\partial u}{\partial x}\right) + \tau_{xy}\left(\frac{\partial u}{\partial y} + \frac{\partial v}{\partial x}\right) + \tau_{yy}\left(\frac{\partial v}{\partial y}\right)\right] = 0, \\
&q_x - k_{xx}\frac{\partial T}{\partial x} - k_{xy}\frac{\partial T}{\partial y} = 0, \\
&q_y - k_{yy}\frac{\partial T}{\partial y} - k_{xy}\frac{\partial T}{\partial x} = 0, \\
&Re_n = \frac{\rho_0 v_0^{2-n} L^n}{m_0}, \\
&Pr_n = \frac{C_{p_0} m_0}{k_0}\left(\frac{v_0}{L}\right)^{n-1}, \\
&Br_n = \frac{m_0 v_0^{n+1}}{k_0(T_1 - T_0)L^{n-1}},
\end{aligned} \tag{10}
$$

where Re_n, Pr_n, and Br_n are the Reynolds, Prandtl and Brinkman numbers respectively for a power-law fluid.[41] The dimensionless forms of the equations describing the power-law viscosity are

$$\eta_v = \frac{m(T)}{Re_n}(I_2)^{(n-1)/2},$$
$$I_2 = 2\left(\frac{\partial u}{\partial x}\right)^2 + 2\left(\frac{\partial v}{\partial y}\right)^2 + \left(\frac{\partial u}{\partial y} + \frac{\partial v}{\partial x}\right)^2. \tag{11}$$

LSFEF OF THE NON-DIMENSIONAL EQUATIONS OF MOTION AND HEAT TRANSFER

In this formulation P, u, v, τ_{xx}, τ_{xy}, τ_{yy}, T, q_x and q_y are considered to be the dependent or field variables. By considering the stresses and heat fluxes as dependent variables, we obtain a set of coupled first-order non-linear partial differential equations, (10), which permit the use of C^0 approximation functions. Generally P, u, v and T are called primary variables and τ_{xx}, τ_{xy}, τ_{yy}, q_x and q_y are called auxiliary variables.

Element approximation

If we consider the same order of approximation for all the field variables, then we can write

$$\Phi^h = [N]\{\Phi\}, \tag{12}$$

where Φ is the field variable, $[N]$ is the hierarchical approximation function matrix and $\{\Phi\}$ are the hierarchical nodal degrees of freedom for the field variable Φ. By letting $\Phi = P$, u, v, τ_{xx}, τ_{xy}, τ_{yy}, T, q_x, and q_y, we can write the element approximation for each of the nine dependent variables. For example, $P^h = [N]\{P\}$, $u^h = [N]\{u\}$, etc. In the present work we consider a nine-node quadrilateral element with curved sides. The element is mapped on to a two-unit square in the natural co-ordinate space ξ, η (Figure 1). The hierarchical approximation functions and nodal variables are constructed in the natural co-ordinate space ξ, η. Details of this procedure can be found in References 1 and 21 and are omitted here for the sake of brevity.

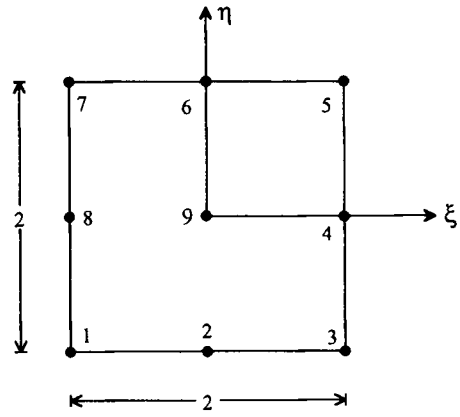

Figure 1. Nine node p-version finite element

When the finite element approximations P^h, u^h, v^h, etc. are substituted into the dimensionless forms of the equations of motion, the resulting errors can be written as

$$
\begin{aligned}
E_1^e &= \frac{\partial u^h}{\partial x} + \frac{\partial v^h}{\partial y},\\
E_2^e &= u^h \frac{\partial u^h}{\partial x} + v^h \frac{\partial u^h}{\partial y} + \frac{\partial P^h}{\partial x} - \left(\frac{\partial \tau_{xx}^h}{\partial x} + \frac{\partial \tau_{xy}^h}{\partial y}\right),\\
E_3^e &= u^h \frac{\partial v^h}{\partial x} + v^h \frac{\partial v^h}{\partial y} + \frac{\partial P^h}{\partial y} - \left(\frac{\partial \tau_{xy}^h}{\partial x} + \frac{\partial \tau_{yy}^h}{\partial y}\right),\\
E_4^e &= \tau_{xx}^h - 2\eta_v \frac{\partial u^h}{\partial x},\\
E_5^e &= \tau_{xy}^h - \eta_v\left(\frac{\partial u^h}{\partial y} + \frac{\partial v^h}{\partial x}\right),\\
E_6^e &= \tau_{yy}^h - 2\eta_v\left(\frac{\partial v^h}{\partial y}\right),\\
E_7^e &= \left(u^h \frac{\partial T^h}{\partial x} + v^h \frac{\partial T^h}{\partial y}\right) - \frac{1}{Re_n Pr_n}\left(\frac{\partial q_x^h}{\partial x} + \frac{\partial q_y^h}{\partial y}\right)\\
&\quad - \frac{Br_n}{Pr_n}\left[\tau_{xx}^h\left(\frac{\partial u^h}{\partial x}\right) + \tau_{xy}^h\left(\frac{\partial u^h}{\partial y} + \frac{\partial v^h}{\partial x}\right) + \tau_{yy}^h\left(\frac{\partial v^h}{\partial y}\right)\right],\\
E_8^e &= q_x^h - k_{xx}\frac{\partial T^h}{\partial x} - k_{xy}\frac{\partial T^h}{\partial y},\\
E_9^e &= q_y^h - k_{yy}\frac{\partial T^h}{\partial y} - k_{xy}\frac{\partial T^h}{\partial x}.
\end{aligned}
\tag{13}
$$

For the second invariant of the rate-of-strain tensor we have

$$
I_2^h = 2\left(\frac{\partial u^h}{\partial x}\right)^2 + 2\left(\frac{\partial v^h}{\partial y}\right)^2 + \left(\frac{\partial u^h}{\partial y} + \frac{\partial v^h}{\partial x}\right)^2. \tag{14}
$$

In addition to the errors given by (13), the LSFEF presented in the previous section requires expressions for the derivatives of the errors with respect to the $\{\delta^e\}$-vector. In this case, if we choose

$$
\{\delta^e\}^T = [\{P\}^T, \{u\}^T, \{v\}^T, \{\tau_{xx}\}^T, \{\tau_{xy}\}^T, \{\tau_{yy}\}^T, \{T\}^T, \{q_x\}^T, \{q_y\}^T], \tag{15}
$$

then

$$
\begin{aligned}
\left\{\frac{\partial E_i^e}{\partial\{\delta^e\}}\right\}^T = \Bigg[&\left\{\frac{\partial E_i^e}{\partial\{P\}}\right\}^T, \left\{\frac{\partial E_i^e}{\partial\{u\}}\right\}^T, \left\{\frac{\partial E_i^e}{\partial\{v\}}\right\}^T, \left\{\frac{\partial E_i^e}{\partial\{\tau_{xx}\}}\right\}^T, \left\{\frac{\partial E_i^e}{\partial\{\tau_{xy}\}}\right\}^T, \left\{\frac{\partial E_i^e}{\partial\{\tau_{yy}\}}\right\}^T,\\
&\left\{\frac{\partial E_i^e}{\partial\{T\}}\right\}^T, \left\{\frac{\partial E_i^e}{\partial\{q_x\}}\right\}^T, \left\{\frac{\partial E_i^e}{\partial\{q_y\}}\right\}^T\Bigg].
\end{aligned}
\tag{16}
$$

Using (12) with $\Phi = P, u, v, \tau_{xx}, \tau_{xy}, \tau_{yy}, T, q_x$ and q_y and the equations for E_i^e, $i = 1, 2, \ldots, 9$, (13), the required expressions in (16) can be obtained easily as

$$\left\{\frac{\partial E_1^e}{\partial\{\delta^e\}}\right\}^{\mathrm{T}} = \left[[0], \left[\frac{\partial N}{\partial x}\right], \left[\frac{\partial N}{\partial y}\right], [0], [0], [0], [0], [0], [0]\right], \tag{17}$$

$$\left\{\frac{\partial E_2^e}{\partial\{\delta^e\}}\right\}^{\mathrm{T}} = \left[\left[\frac{\partial N}{\partial x}\right], u^h\left[\frac{\partial N}{\partial x}\right] + \frac{\partial u^h}{\partial x}[N] + v^h\left[\frac{\partial N}{\partial y}\right], \frac{\partial u^h}{\partial y}[N], -\left[\frac{\partial N}{\partial x}\right], -\left[\frac{\partial N}{\partial y}\right], [0], [0], [0], [0]\right], \tag{18}$$

$$\left\{\frac{\partial E_3^e}{\partial\{\delta^e\}}\right\}^{\mathrm{T}} = \left[\left[\frac{\partial N}{\partial y}\right], \frac{\partial v^h}{\partial x}[N], u^h\left[\frac{\partial N}{\partial x}\right] + v^h\left[\frac{\partial N}{\partial y}\right] + \frac{\partial v^h}{\partial y}[N], [0], -\left[\frac{\partial N}{\partial x}\right], -\left[\frac{\partial N}{\partial y}\right], [0], [0], [0]\right], \tag{19}$$

$$\left\{\frac{\partial E_4^e}{\partial\{\delta^e\}}\right\}^{\mathrm{T}} = \left[[0], -2\eta_v\left[\frac{\partial N}{\partial x}\right] - 2\frac{\partial u^h}{\partial x}\left\{\frac{\partial \eta_v}{\partial\{u\}}\right\}^{\mathrm{T}}, -2\frac{\partial u^h}{\partial x}\left\{\frac{\partial \eta_v}{\partial\{v\}}\right\}^{\mathrm{T}}, [N], [0], [0], -2\frac{\partial u^h}{\partial x}\left\{\frac{\partial \eta_v}{\partial\{T\}}\right\}^{\mathrm{T}}, [0], [0]\right], \tag{20}$$

$$\left\{\frac{\partial E_5^e}{\partial\{\delta^e\}}\right\}^{\mathrm{T}} = \left[[0], -\eta_v\left[\frac{\partial N}{\partial y}\right] - \left(\frac{\partial u^h}{\partial y} + \frac{\partial v^h}{\partial x}\right)\left\{\frac{\partial \eta_v}{\partial\{u\}}\right\}^{\mathrm{T}}, -\eta_v\left[\frac{\partial N}{\partial x}\right] - \left(\frac{\partial u^h}{\partial y} + \frac{\partial v^h}{\partial x}\right)\left\{\frac{\partial \eta_v}{\partial\{v\}}\right\}^{\mathrm{T}}, [0], [N], [0], -\left(\frac{\partial u^h}{\partial y} + \frac{\partial v^h}{\partial x}\right)\left\{\frac{\partial \eta_v}{\partial\{T\}}\right\}^{\mathrm{T}}, [0], [0]\right], \tag{21}$$

$$\left\{\frac{\partial E_6^e}{\partial\{\delta^e\}}\right\}^{\mathrm{T}} = \left[[0], -2\frac{\partial v^h}{\partial y}\left\{\frac{\partial \eta_v}{\partial\{u\}}\right\}^{\mathrm{T}}, -2\eta_v\left[\frac{\partial N}{\partial y}\right] - 2\frac{\partial v^h}{\partial y}\left\{\frac{\partial \eta_v}{\partial\{v\}}\right\}^{\mathrm{T}}, [0], [0], [N], -2\frac{\partial v^h}{\partial y}\left\{\frac{\partial \eta_v}{\partial\{T\}}\right\}^{\mathrm{T}}, [0], [0]\right], \tag{22}$$

$$\left\{\frac{\partial E_7^e}{\partial\{\delta^e\}}\right\}^{\mathrm{T}} = \left[[0], \frac{\partial T^h}{\partial x}[N] - \frac{Br_n}{Pr_n}\left(\tau_{xx}^h\left[\frac{\partial N}{\partial x}\right] + \tau_{xy}^h\left[\frac{\partial N}{\partial y}\right]\right), \frac{\partial T^h}{\partial y}[N] - \frac{Br_n}{Pr_n}\left(\tau_{xy}^h\left[\frac{\partial N}{\partial x}\right] + \tau_{yy}^h\left[\frac{\partial N}{\partial y}\right]\right), -\frac{Br_n}{Pr_n}\frac{\partial u^h}{\partial x}[N], -\frac{Br_n}{Pr_n}\left(\frac{\partial u^h}{\partial y} + \frac{\partial v^h}{\partial x}\right)[N], -\frac{Br_n}{Pr_n}\frac{\partial v^h}{\partial y}[N], u^h\left[\frac{\partial N}{\partial x}\right] + v^h\left[\frac{\partial N}{\partial y}\right], -\frac{1}{Re_n Pr_n}\left[\frac{\partial N}{\partial x}\right], -\frac{1}{Re_n Pr_n}\left[\frac{\partial N}{\partial y}\right]\right], \tag{23}$$

$$\left\{\frac{\partial E_8^e}{\partial\{\delta^e\}}\right\}^{\mathrm{T}} = \left[[0], [0], [0], [0], [0], [0], -k_{xx}\left[\frac{\partial N}{\partial x}\right] - \frac{\partial T^h}{\partial x}\left\{\frac{\partial k_{xx}}{\partial\{T\}}\right\}^{\mathrm{T}} - k_{xy}\left[\frac{\partial N}{\partial y}\right] - \frac{\partial T^h}{\partial y}\left\{\frac{\partial k_{xy}}{\partial\{T\}}\right\}^{\mathrm{T}}, [N], [0]\right], \tag{24}$$

$$\left\{\frac{\partial E_9^e}{\partial\{\delta^e\}}\right\}^{\mathrm{T}} = \left[[0], [0], [0], [0], [0], [0], -k_{xy}\left[\frac{\partial N}{\partial x}\right] - \frac{\partial T^h}{\partial x}\left\{\frac{\partial k_{xy}}{\partial\{T\}}\right\}^{\mathrm{T}} - k_{yy}\left[\frac{\partial N}{\partial y}\right] - \frac{\partial T^h}{\partial y}\left\{\frac{\partial k_{yy}}{\partial\{T\}}\right\}^{\mathrm{T}}, [0], [N]\right]. \tag{25}$$

The derivatives of η_v with respect to $\{u\}$, $\{v\}$ and $\{T\}$ appearing in the expressions for the partial derivatives of E_i^e with respect to $\{\delta^e\}$ can be easily obtained using (11) and (14) as

$$\begin{aligned}
\left\{\frac{\partial \eta_v}{\partial\{u\}}\right\} &= \frac{m(T)}{Re_n}\frac{n-1}{2}(I_2^h)^{(n-3)/2}\left\{\frac{\partial I_2^h}{\partial\{u\}}\right\},\\
\left\{\frac{\partial \eta_v}{\partial\{v\}}\right\} &= \frac{m(T)}{Re_n}\frac{n-1}{2}(I_2^h)^{(n-3)/2}\left\{\frac{\partial I_2^h}{\partial\{v\}}\right\},\\
\left\{\frac{\partial \eta_v}{\partial\{T\}}\right\} &= \frac{1}{Re_n}(I_2^h)^{(n-1)/2}\left(\frac{\partial m}{\partial T}\right)\left\{\frac{\partial T}{\partial\{T\}}\right\},
\end{aligned} \tag{26}$$

where

$$\begin{aligned}
\left\{\frac{\partial I_2^h}{\partial\{u\}}\right\} &= 4\frac{\partial u^h}{\partial x}\left[\frac{\partial N}{\partial x}\right]^T + 2\left(\frac{\partial u^h}{\partial y}+\frac{\partial v^h}{\partial x}\right)\left[\frac{\partial N}{\partial y}\right]^T,\\
\left\{\frac{\partial I_2^h}{\partial\{v\}}\right\} &= 4\frac{\partial v^h}{\partial y}\left[\frac{\partial N}{\partial y}\right]^T + 2\left(\frac{\partial u^h}{\partial y}+\frac{\partial v^h}{\partial x}\right)\left[\frac{\partial N}{\partial x}\right]^T,\\
\left\{\frac{\partial T}{\partial\{T\}}\right\} &= [N]^T.
\end{aligned} \tag{27}$$

We also note that

$$\left\{\frac{\partial k_{ij}}{\partial\{T\}}\right\} = \frac{\partial k_{ij}}{\partial T}\frac{\partial T}{\partial\{T\}} = \frac{\partial k_{ij}}{\partial T}[N]^T, \quad i,j = x, y.$$

Knowing the explicit forms of $k_{ij} = k_{uj}(T)$, $\partial k_{ij}/\partial T$ can be easily computed.

Note that equations (13), (24) and (25) are written for the general case of an anisotropic fluid with temperature-dependent thermal conductivities. In the numerical examples we assume $k_{xy} = 0$ and $k_{xx} = k_{yy}$ and we consider the thermal conductivity to be independent of temperature.

The errors given by equation (13) and the derivatives of the errors with respect to the degrees of freedom vector $\{\delta^e\}$ given by equations (17)–(25) are used to compute $\{g^e\}$ defined in equation (2) and the Hessian matrix $[H^e]$ defined in equation (4). The numerical values of the integrals are calculated exactly using Gaussian quadrature with a '$2p + 1$ integration rule' in both ξ and η natural co-ordinate directions, where p is the order of the polynomial approximation.

Remarks

The importance of the choice of the non-dimensional form can be examined more closely by considering its effect on the LSFEF. In the least squares process we minimize the sum of squares of the errors given by equation (1). In this process the relative importance of the individual equations can be altered through the use of weight factors.[9,43,44] If one or more equations in the set are weighted more heavily than the others, the minimization process is forced to satisfy these equations at the expense of the rest. The non-dimensional forms of the constitutive equations resulting from the two choices of the characteristic scale for the stresses represent the same equations but with different weight factors.

The values of the errors resulting from the stress equations using the characteristic viscous stress scale are always a factor of Re_n times greater than those resulting from the characteristic kinetic energy scale. This means that for a given problem, as the Reynolds number is increased,

the relative weighting on the stress equations increases when the characteristic viscous stress scale is used. As the Reynolds number is increased, the magnitude of the velocity gradients increases throughout the flow field. When the characteristic kinetic energy is used to scale the stresses, the ratio of the magnitude of the velocity gradients and the Reynolds number (which appears in the stress equations for this scale) remains approximately constant. This has the effect of maintaining a constant weight factor for the stress equations as the Reynolds number is changed. In the present study the increased weighting on the stress equations associated with the characteristic viscous stress scale was found to be very undesirable, leading to non-convergence or convergence to spurious solutions for a variety of problems even at low to moderate Reynolds numbers. A numerical example is presented in the next section to illustrate this point.

With these observations in mind, the generalization can be made that when using non-dimensionalized equations in the least squares process, the non-dimensional form should be chosen such that the relative weight of each equation is not strongly affected by the value of any non-dimensional parameter contained in the equations.

LSFEF for isothermal case

For isothermal flow the energy equation and the heat flux equations do not participate and thus for the element error equations in (13) we have E_i, $i = 1, 2, \ldots, 6$, and the temperature T and heat fluxes q_x and q_y are no longer field variables. For this case the element nodal degrees of freedom vector reduces to $\{\delta^e\}^T = [\{P\}^T, \{u\}^T, \{v\}^T, \{\tau_{xx}\}^T, \{\tau_{xy}\}^T, \{\tau_{yy}\}^T]$. Naturally in this case the viscosity (η_v) is not a function of temperature. Thus m in equation (11) is not a function of temperature.

NUMERICAL EXAMPLES

In this section numerical examples are presented for isothermal as well as non-isothermal non-Newtonian fluid flow using the power-law model for viscosity to demonstrate the accuracy and convergence characteristics of the present p-version least squares finite element formulation. The numerical examples for isothermal flow consist of fully developed flow between parallel plates, flow in a 2:1 symmetric sudden expansion and flow in a lid-driven cavity. For non-isothermal flow the numerical examples include Couette shear flow and flow in a 4:1 symmetric sudden contraction. The system of algebraic equations in (3) is solved using the wavefront method.[1]

Example 1. Fully developed flow between parallel plates (isothermal flow)

The fully developed flow of a power-law fluid, unlike that of a Newtonian fluid, represents a non-linear problem. The degree of non-linearity increases as the power-law index deviates from unity. Figure 2 shows the region modelled using one and three p-version elements. Because of symmetry, we need only consider the upper (or lower) half of the cross-section.

The analytical solution for the velocity profile is given by

$$u = \frac{\hat{u}}{u_{avg}} = \frac{2n+1}{n+1}(1 - y^{(n+1)/n}). \tag{28}$$

Figure 3 shows a plot of the error functional I versus degrees of freedom (DOF) when the three-element model was used for $n = 0{\cdot}75$ and $1{\cdot}50$. The solutions for $n = 1{\cdot}0$ and $0{\cdot}5$ match

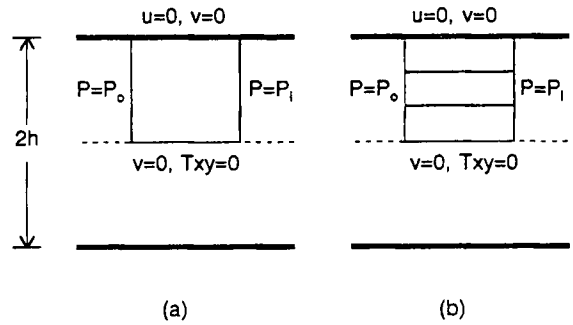

Figure 2. Schematic and finite element models for pressure-driven fully developed flow (Example 1): (a) one-element model: (b) three-element model

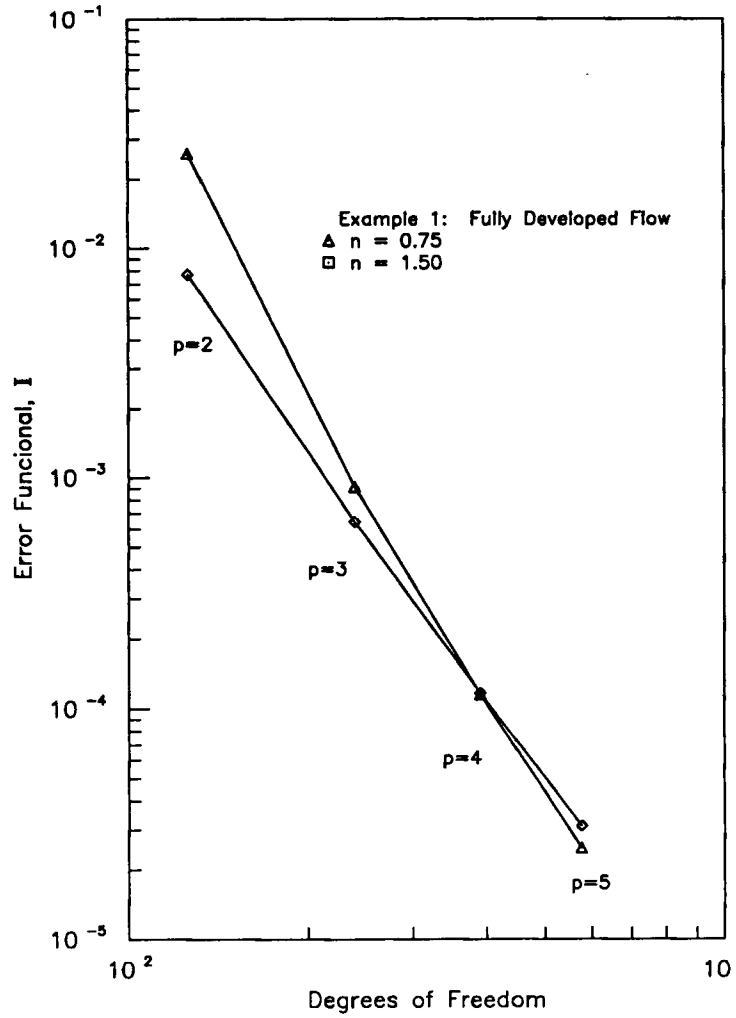

Figure 3. p-Convergence of the error functional I for $n = 0{\cdot}75$ and $1{\cdot}5$—three-element model (Example 1)

the analytical solution exactly and were obtained using a one-element model with $p = 2$ and 3 respectively. For $n < 0{\cdot}5$ and $n > 1{\cdot}5$ a simple continuation procedure in the power-law index was needed. A uniform mesh consisting of three elements was adequate. For $n < 0{\cdot}5$ the converged solution at $n = 0{\cdot}5$ was used as the starting solution, whereas for $n > 1{\cdot}5$ the converged solution at $n = 1{\cdot}5$ was used as the starting solution. No more than two steps in n were required to obtain an accurate solution.

A continuation method in the power-law index is required for extreme values of n, because Newton's solution procedure requires a starting solution within a small neighbourhood of the true solution to ensure convergence. For $n < 0{\cdot}5$ and $n > 1{\cdot}5$ the initial starting solution ($\{\delta_0\} = \{0\}$ and $n = 1{\cdot}0$) is far from being within a small neighbourhood of the true solution. However, for $0{\cdot}5 \leq n \leq 1{\cdot}5$, $\{\delta_0\} = \{0\}$ and $n = 1{\cdot}0$ serves as a good starting solution and results in satisfactory convergence of Newton's method. Furthermore, whenever a good starting solution was used, the number of iterations required by Newton's method was always seven or less. This was true for all numerical examples presented in this paper. A convergence tolerance of less than or equal to 10^{-4} was used for both $\{g\}$ and I.

We note that the range of power-law index n for which $\{\delta_0\} = \{0\}$ and $n = 1{\cdot}0$ serves as a good starting solution if the solution is problem-dependent. For Examples 2 and 3, $n = 1{\cdot}0$ served as a good starting solution and continuation in the power-law index was not required. The converged velocity profiles obtained from the present formulation show excellent agreement with the analytical solution (Figure 4).

Example 2. A 2 : 1 symmetric sudden expansion (isothermal flow)

The flow in a 2:1 symmetric sudden expansion is characterized by fully developed flow at the inlet and exit and a region of recirculation in the corner just after the expansion. Figure 5(a) shows a schematic of the problem with the boundary conditions and Figure 5(b) shows a graded 26 p-version finite element mesh. The element sizes and the mesh details near the corner are shown in Figure 5(c).

The Reynolds number in this case is defined as $Re_n = \rho_0 u_{\text{avg}}^{2-n} s^n / m_0$, where u_{avg} is the average inlet velocity and s is the step height. No-slip conditions were applied at the walls and symmetry conditions of flow were enforced at the centreline by specifying the shear stress and vertical velocity to be zero there. A fully developed velocity profile, scaled to represent a unit flow rate, was specified at the inlet and the pressure was specified at one node on the centreline at the entrance. Conditions of fully developed flow were applied at the exit by specifying $\tau_{xx} = 0$ and $v = 0$.

The finite element mesh was finely graded near the corner because of the sharp gradients of velocity and pressure in this region. A Reynolds number of 10 was used in all cases, while the power-law index was varied between 0·25 and 1·5. This value of Re_n was selected to ensure that both sources of non-linearity (convection and viscous terms) were important and to concentrate on the changes in the flow behaviour due to changes in n. The 26-element graded mesh shown in Figure 5(b) was satisfactory for all values of n. Results were computed for a coarse mesh and successive mesh refinements were made based on the element error functional values to arrive at the present 26-element mesh. Figure 6 shows a plot of the error functional versus DOF for various values of n ranging from 0·25 to 1·50 on a log–log scale. The degrees of freedom were increased for the fixed 26-element mesh by uniform p-refinement ($p_\xi = p_\eta = p$) for each element. We note that there was a substantial decrease in the error functional when the p-level was increased from two to five (647 DOF to 4011 DOF). The solution was essentially converged at p-level five for $n \leq 1{\cdot}0$. For $n = 1{\cdot}5$ a higher p-level was needed for convergence. We also note

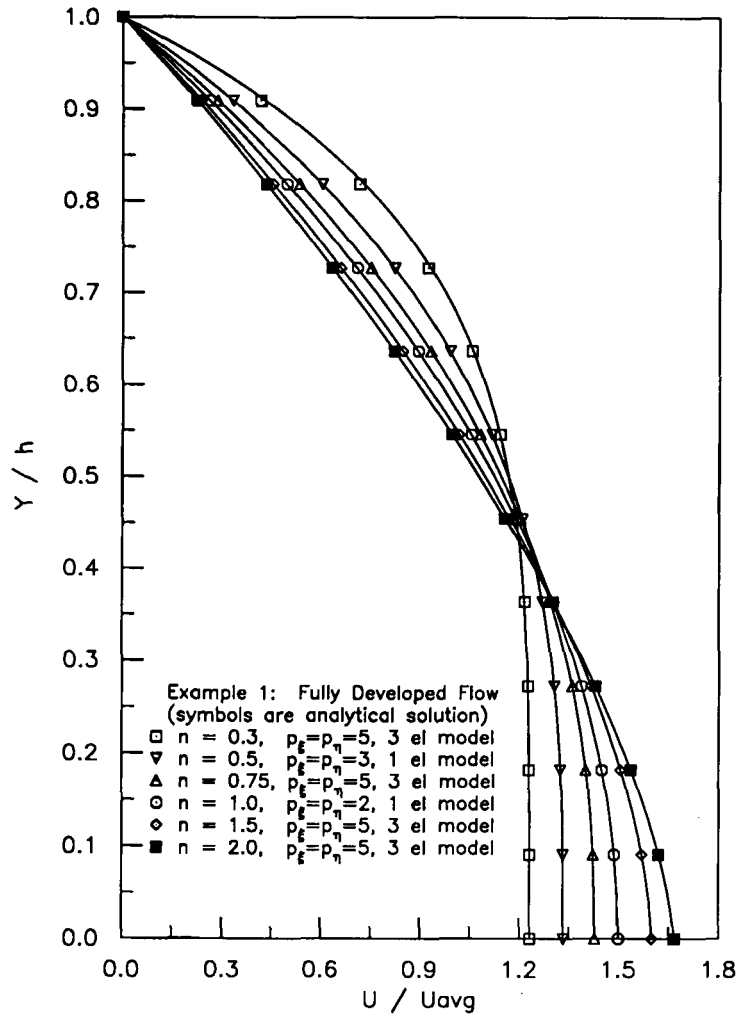

Figure 4. Velocity profiles for various values of the power-law index (Example 1)

that the rate of convergence was essentially the same for all values of n except 0·25. For $n = 0{\cdot}25$ the rate of convergence was greater between p-levels three and seven. The number of iterations required was less than seven for a convergence tolerance of less than or equal to 10^{-4} for both $\{g\}$ and I.

Figures 7(a)–7(c) show streamline plots for power-law indices of 0·25, 1·0 and 1·5 respectively. It can be seen that the size of the vortex and the maximum streamline value in the vortex increase as the power-law index is increased. The maximum value of the streamfunction in the vortex for the Newtonian flow (Figure 7(b)) was 1·0126, which is very close to the value of 1·0124 reported by Georgiou *et al.*[45] for this problem. The converged horizontal velocity profiles at various locations for $n = 0{\cdot}25$, 1·0 and 1·25 are shown in Figures 8–10. For this Reynolds number $x/s = 20$ was a sufficient length to obtain fully developed flow at the exit. In Figures 8–10 the circles represent the fully developed analytical solution for flow between parallel plates. Our calculated exit velocity profiles are in excellent agreement with the analytical solution. Extremely

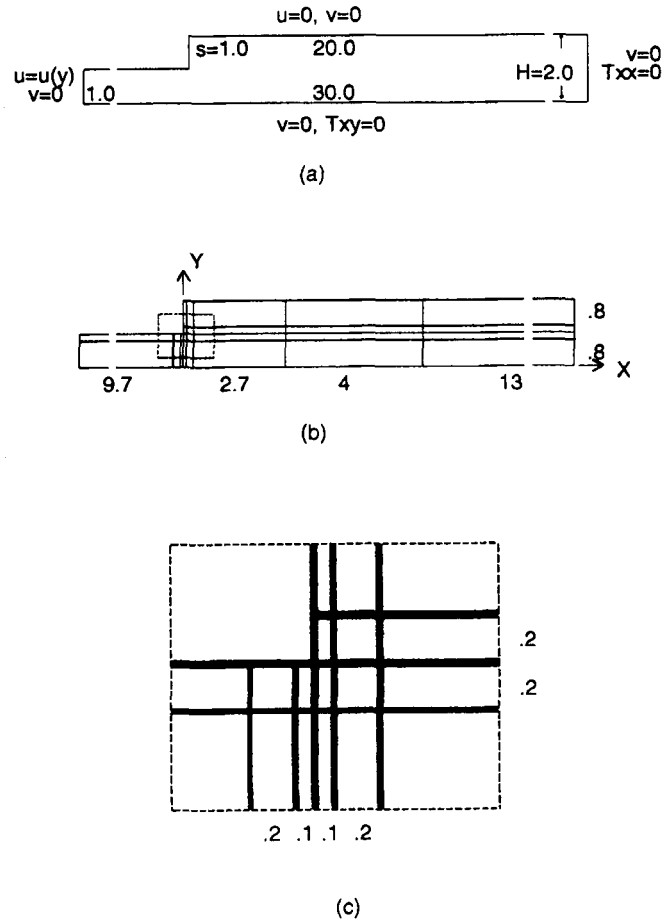

Figure 5. Schematic and finite element model for the 2:1 symmetric sudden expansion (Example 2): (a) schematic and boundary conditions; (b) 26-element graded mesh showing element lengths; (c) finite element mesh details near the corner

low values of the error functional (of the order of 10^{-4} or lower) are an indication of the good accuracy of the velocity profiles at other values of x/s as well as the good accuracy of the other field variables.

The skin friction coefficient along the wall ($c_f = 2(\tau_{xy})_{wall}/\rho_0 u_{avg}^2$) downstream of the expansion is plotted in Figure 11 for various values of n. The initial 'dip' in the curves signifies the region of recirculation where the flow is directed backwards. The position downstream where $c_f = 0$ is the point of reattachment of the flow. Figure 12 is a plot of the reattachment length (x_r) as a function of the power-law index n. We note that x_r decreases as n decreases, which is in agreement with results reported by others for similar problems.[24,34] A pressure contour plot for a Newtonian flow is given in Figure 13. The location of minimum pressure is on the vertical wall very near the corner of the expansion. Pressure contour plots for other values of the power-law index in the range $0{\cdot}25 \leq n \leq 1{\cdot}5$ are similar in appearance.

To demonstrate the importance of the choice of the non-dimensional form of the equations of motion, we computed the flow field for $n = 1{\cdot}0$ using the characteristic viscous stress to scale the stresses and compared the results with those obtained using the characteristic kinetic energy

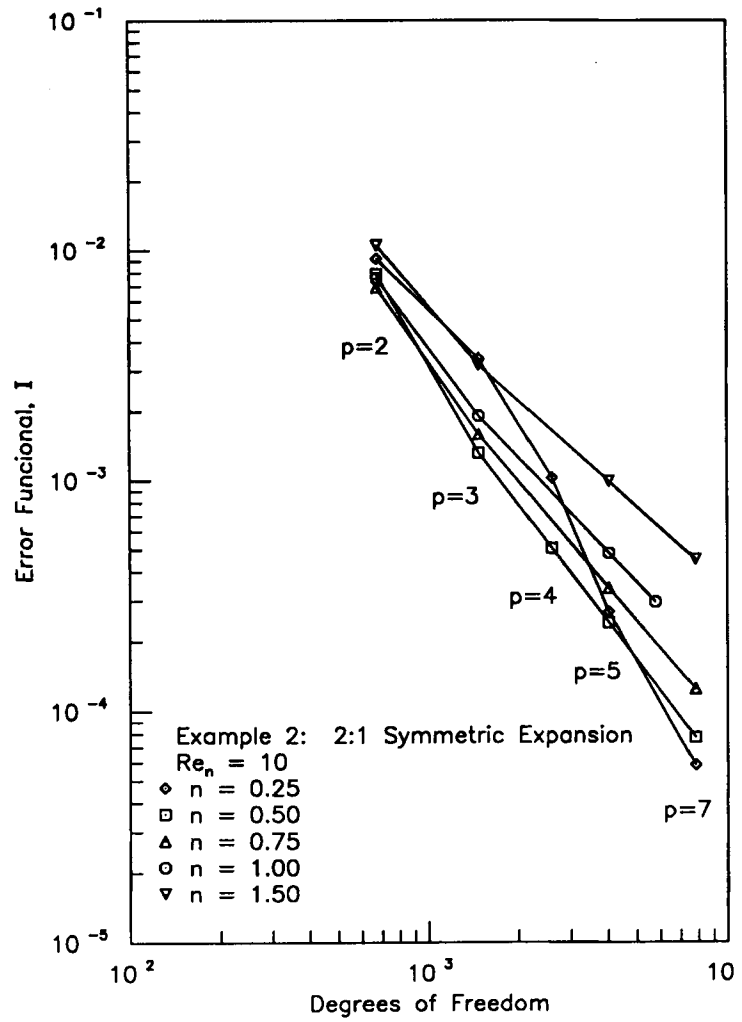

Figure 6. p-Convergence of the error functional I for various values of the power-law index (Example 2)

scale. From Figure 14, which shows a plot of I versus DOF on a log–log scale, it is clear that the characteristic kinetic energy scale resulted in a greater rate of convergence. The hoizontal velocity profiles at various locations for $n = 1{\cdot}0$, calculated using the characteristic viscous stress scale, are shown in Figure 15. Note that in this case the formulation failed to accurately predict the exit velocity profile even when using a higher p-level than that needed to obtain converged results with the characteristic kinetic energy scale. It is obvious that the characteristic kinetic energy scale, for which the Reynolds number appears in the stress equations, is a better choice.

Example 3. Lid-driven cavity (isothermal flow)

The 'lid-driven' cavity has become a standard test problem in computational fluid dynamics. The problem is characterized by a square cavity in which the driving force for the flow is the shear created by the sliding lid. Figure 16 shows a schematic of the cavity with the boundary conditions and the finite element discretization.

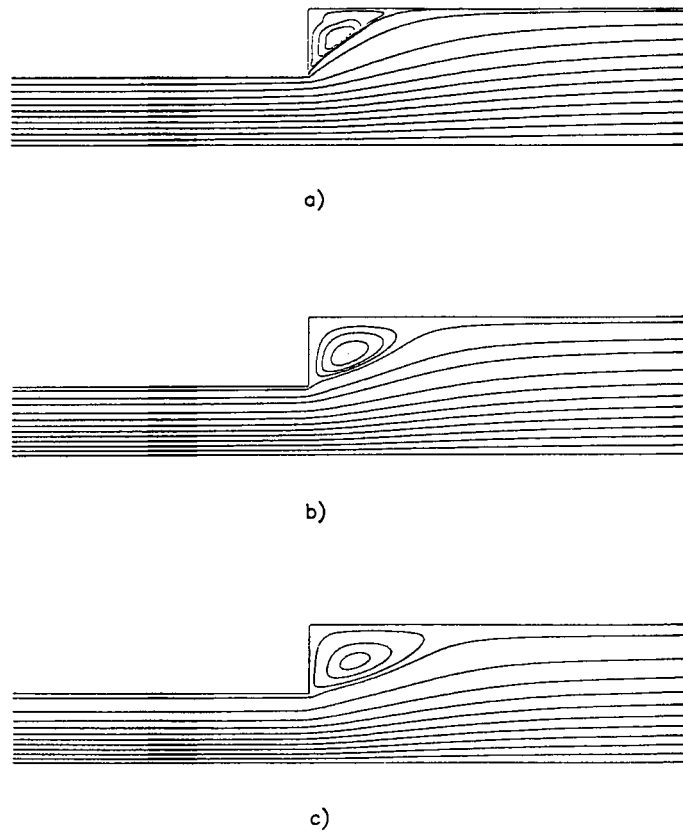

Figure 7. Streamline plots for the 2:1 symmetric sudden expansion for power law indices of (a) 0·25, (b) 1·0 and (c) 1·5. The maximum streamfunction values in the vortex are 1·00006, 1·0126 and 1·0226 respectively. In all cases $Re_n = 10$ and $-4 \leq x \leq 5$

The Reynolds number for this problem is defined as $Re_n = \rho_0 u_0^{2-n} D^n / m_0$, where u_0 is the velocity of the lid and D is the dimension of the cavity. The Reynolds number was chosen to be 100 and was kept constant, while the value of the power-law index was varied from 0·25 to 1·5. The 25-element model was found to be adequate for all values of n. This was confirmed by further refining the mesh and observing no appreciable change in the error functional or in the primary and auxiliary variables. Figure 17 shows plots of the error functional versus DOF for $n = 0{\cdot}25$ and 1·5. Plots for $0{\cdot}25 < n < 1{\cdot}5$ were similar and fell between the graphs for $n = 0{\cdot}25$ and 1·5. The velocities, pressure and auxiliary variables were converged at a p-level of five. The number of iterations required was less than seven for a convergence tolerance less than or equal to 10^{-5} for both $\{g\}$ and I for all cases presented here.

Streamline plots are shown in Figures 18(a)–18(c) for power-law indices of 0·25, 1·0 and 1·5 respectively. From these plots we note that the position of the main vortex shifts towards the upper right corner as the power-law index decreases. Also, the maximum streamline value in the main and corner vortices decreases as n decreases. The streamline pattern for $n = 1{\cdot}0$ (Figure 18(b)) agrees closely with the results reported by Schneider and Raw.[46] The converged horizontal velocity (at a p-level of seven) along the vertical centreline of the cavity is plotted in Figure 19 for various values of n. The solid curve represents the solution for a Newtonian fluid ($n = 1{\cdot}0$)

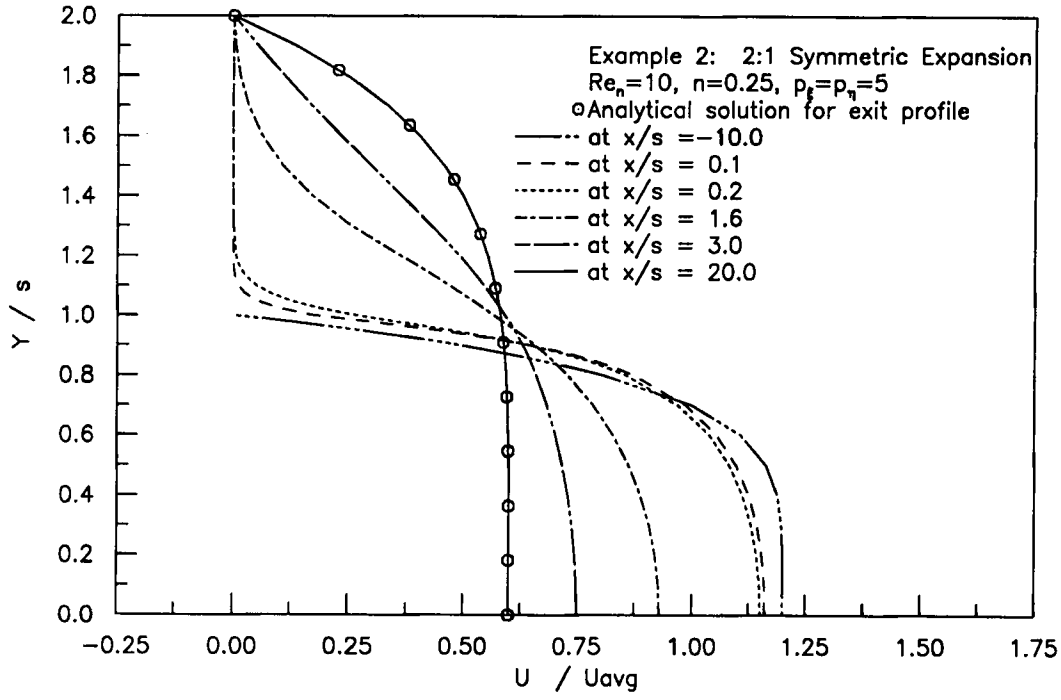

Figure 8. Converged horizontal velocity (u) profiles at various cross-sections for $n = 0{\cdot}25$ (Example 2)

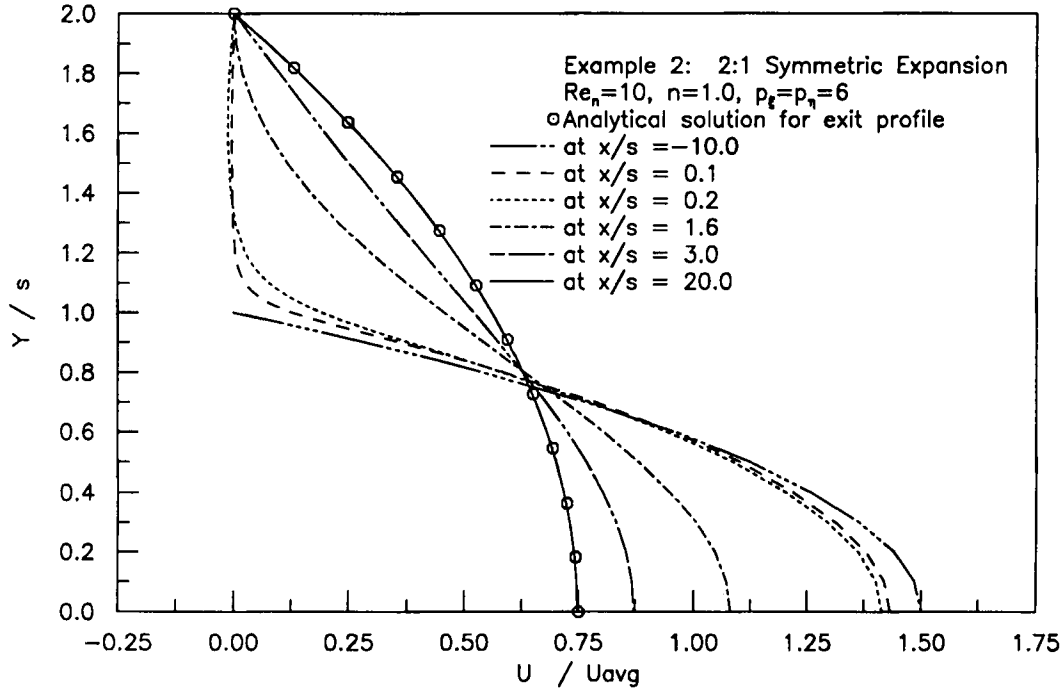

Figure 9. Converged horizontal velocity (u) profiles at various cross-sections for $n = 1{\cdot}0$ (Example 2)

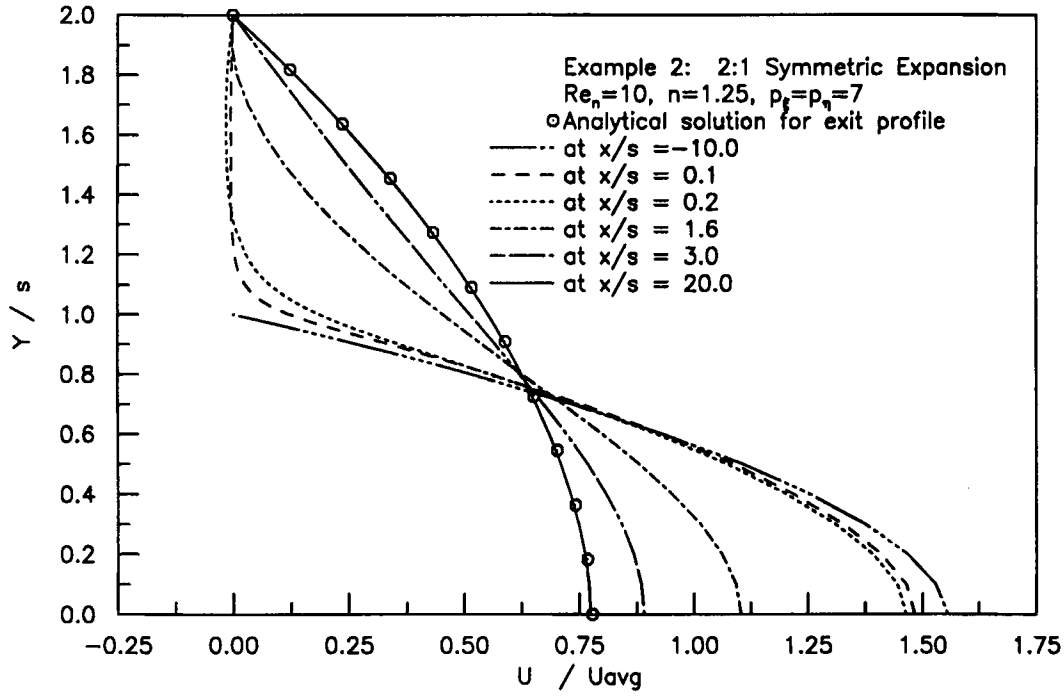

Figure 10. Converged horizontal velocity (u) profiles at various cross-sections for $n = 1{\cdot}25$ (Example 2)

and is compared with results published by Gartling[22] and Ghia *et al.*[47] It can be seen that our calculated solution shows good agreement with these published results. Figure 20 shows the converged vertical velocity profiles along the horizontal centreline of the cavity. As the value of n decreases, the velocity profile becomes flatter, indicating a decreasing circulation in the bottom half of the cavity.

Example 4. Couette shear flow (non-isothermal flow)

This well-known problem is used to verify the accuracy of the current formulation, with particular interest in the solution of the fully coupled energy equation. We consider non-isothermal Newtonian and non-Newtonian flow between parallel walls, with one wall fixed and the other moving with constant unit velocity in the x-direction. A schematic of the problem showing the boundary conditions and a three-element uniform mesh is presented in Figure 21. No-slip conditions are applied at the walls and a zero pressure drop is specified in the flow direction. The walls are held at zero temperature, with heat being generated in the flow by viscous dissipation.

For both Newtonian and non-Newtonian cases the viscosity is considered to be temperature-dependent and the Brinkman number, which scales the viscous dissipation term, is selected to be high enough to cause significant changes in the viscosity. The temperature dependence of the viscosity for a power-law fluid is usually described by considering the temperature dependence of $\hat{m}$ and n separately, but since the temperature dependence of n is negligible for most fluids, only the change in $\hat{m}$ with temperature will be considered. In this example we consider the following relation for $\hat{m}$:[42]

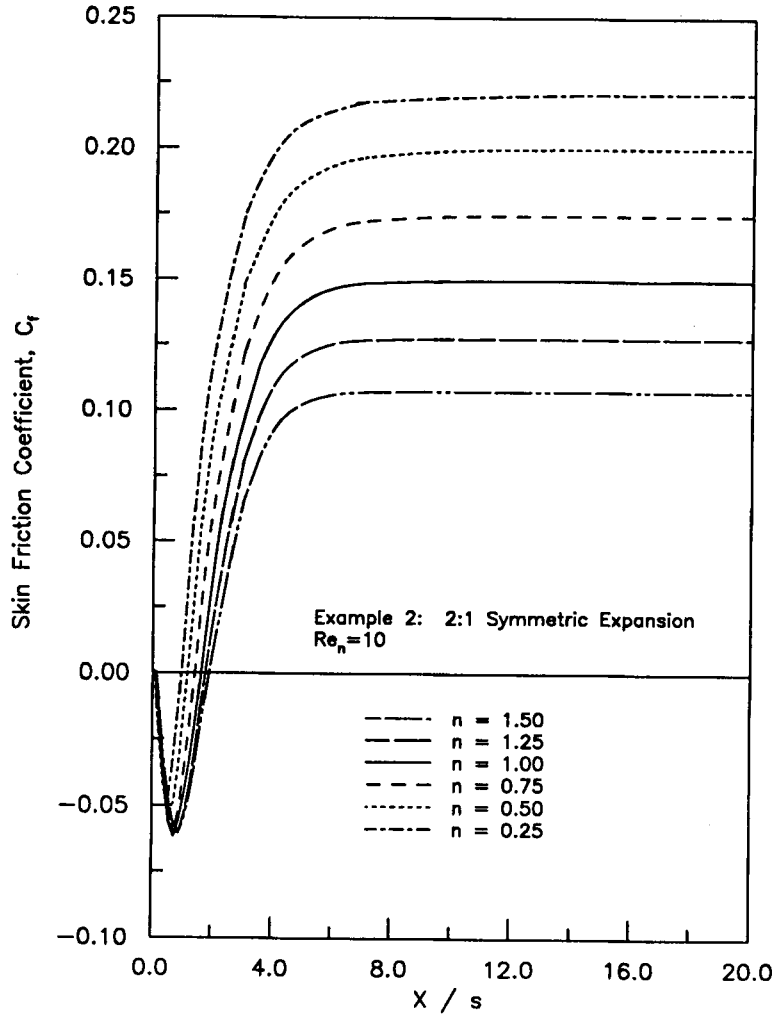

Figure 11. Skin friction coefficient (c_f) along the wall following the expansion for various values of the power-law index (Example 2)

$$\hat{m} = \hat{m}_0 e^{-A(\hat{T}-T_0)/(T_1-T_0)}, \tag{29}$$

where T_1 and T_0 are reference temperatures, $\hat{m}_0$ is the value of the consistency at temperature T_0 and A is the reciprocal characteristic temperature difference of the fluid. The dimensionless form of equation (29) is

$$m = e^{-AT} \tag{30}$$

and thus the derivative of m with respect to T can be written as

$$(\partial m/\partial T) = -Ae^{-AT}. \tag{31}$$

The LSFEF of the non-dimensional equations of motion can now be completed by using equations (30) and (31) in equations (26).

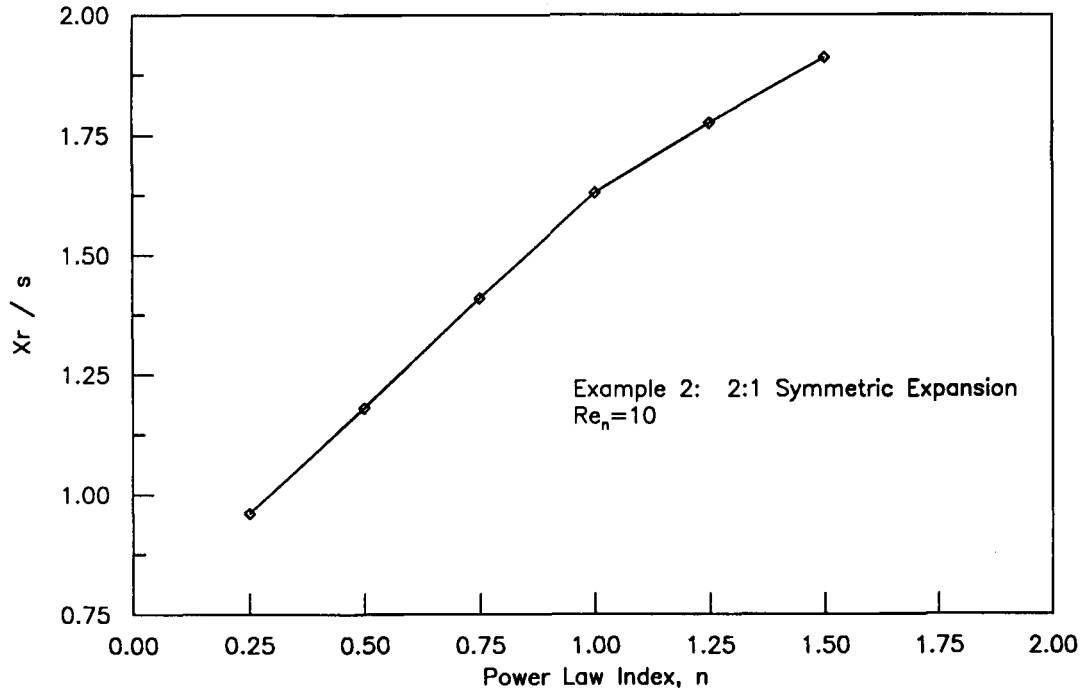

Figure 12. Reattachment length (x_r) as a function of the power-law index (Example 2)

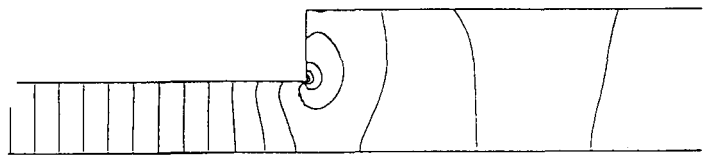

Figure 13. Pressure contour plot for the 2:1 symmetric sudden expansion for $n = 1{\cdot}0$, $Re_n = 10$ and $-4 \leqslant x \leqslant 5$

Here we present results for two cases: case A, a Newtonian fluid with $A = 1{\cdot}0$ and $Br = 100{\cdot}0$; case B, a power-law fluid ($n = 0{\cdot}25$) with $A = 0{\cdot}1$ and $Br_n = 25{\cdot}0$. Since the dependent variables for this problem do not change in the x-direction, the p-level in the ξ-direction is kept fixed at a value of two, while the p-level in the η-direction (y-direction) is varied. Figure 22 shows the p-convergence of the error functional for both cases A and B. We note a smooth monotonic behaviour for both Newtonian and power-law fluids with approximately the same convergence rate. Figures 23 and 24 show the converged velocity profiles and temperature distributions respectively for cases A and B. In both figures the analytical solution published by Turian and Bird[28,29] is given for comparison. Our results show excellent agreement with the analytical solution. The maximum number of iterations was less than seven for a convergence tolerance of 10^{-9} for both $\{g\}$ and I.

The effect of the temperature-dependent viscosity can be clearly seen by observing the departure of the velocity profiles from a straight line in Figure 23. A straight line velocity profile would result if the flow were isothermal or if the viscosity was considered to be independent of temperature.

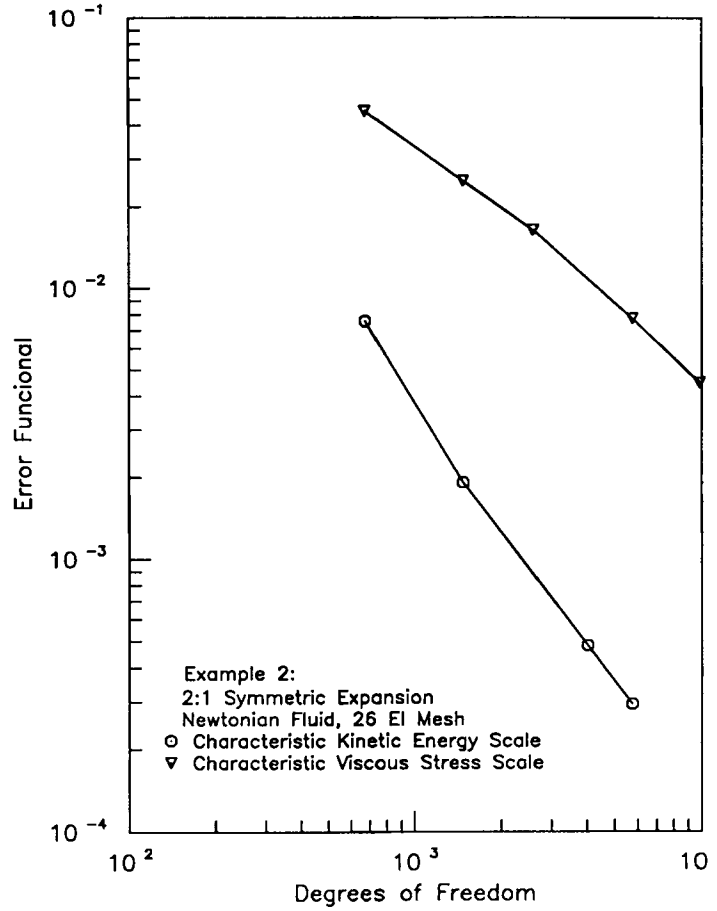

Figure 14. Comparison of the p-convergence characteristics for the two non-dimensional forms (Example 2)

Example 5. A 4 : 1 symmetric sudden contraction (non-isothermal flow)

The numerical simulation of the flow in a 4:1 contraction represents a relatively difficult benchmark problem. Here we examine the accuracy and convergence characteristics of the current formulation for this problem by simulating the non-isothermal flow of Newtonian and power-law fluids with a temperature-dependent viscosity. Viscous dissipation is the source of heat generation.

Figure 25(a) shows a schematic of the problem with the boundary conditions and Figure 25(b) shows a graded 132 p-version finite element mesh. No-slip conditions and zero temperature were specified along the wall. Along the centreline the vertical velocity, shear stress and heat flux in the y-direction were all set to zero. The inlet conditions were specified to represent fully developed flow between parallel plates with a unit flow rate and temperature-independent viscosity. The analytical expressions for the velocity and temperature profiles of a power-law fluid under these conditions are

$$u = \frac{1}{\beta}\frac{2n+1}{n+1}\left[1 - \left(\frac{y}{\beta}\right)^{(n+1)/n}\right] \tag{32}$$

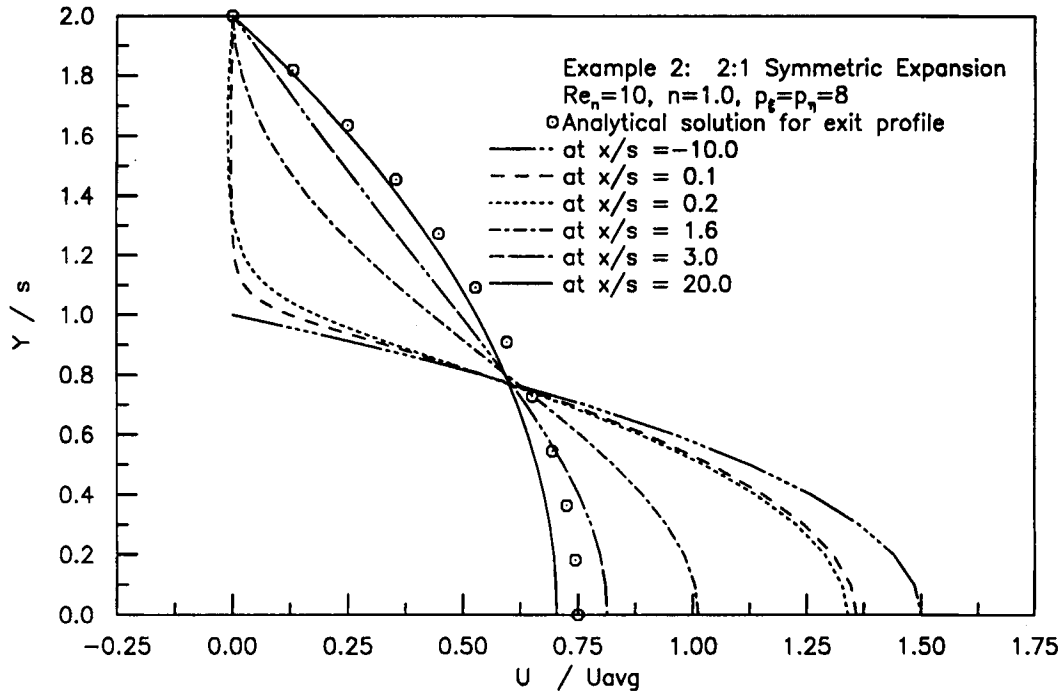

Figure 15. Converged horizontal velocity (u) profiles for $n = 1{\cdot}0$ using the 'characteristic viscous stress' to scale the stresses (Example 2)

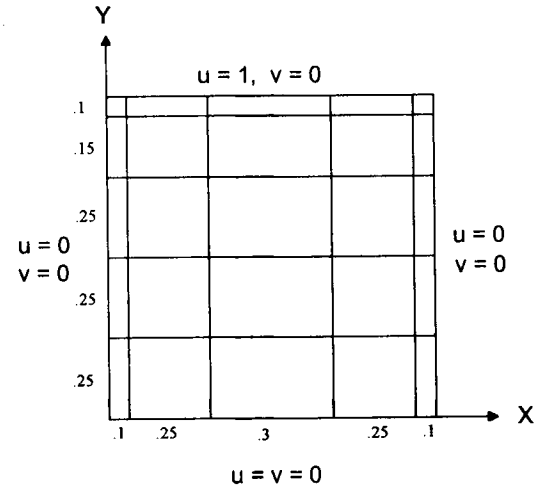

Figure 16. Graded 25-element model for the lid-driven cavity showing boundary conditions and element lengths

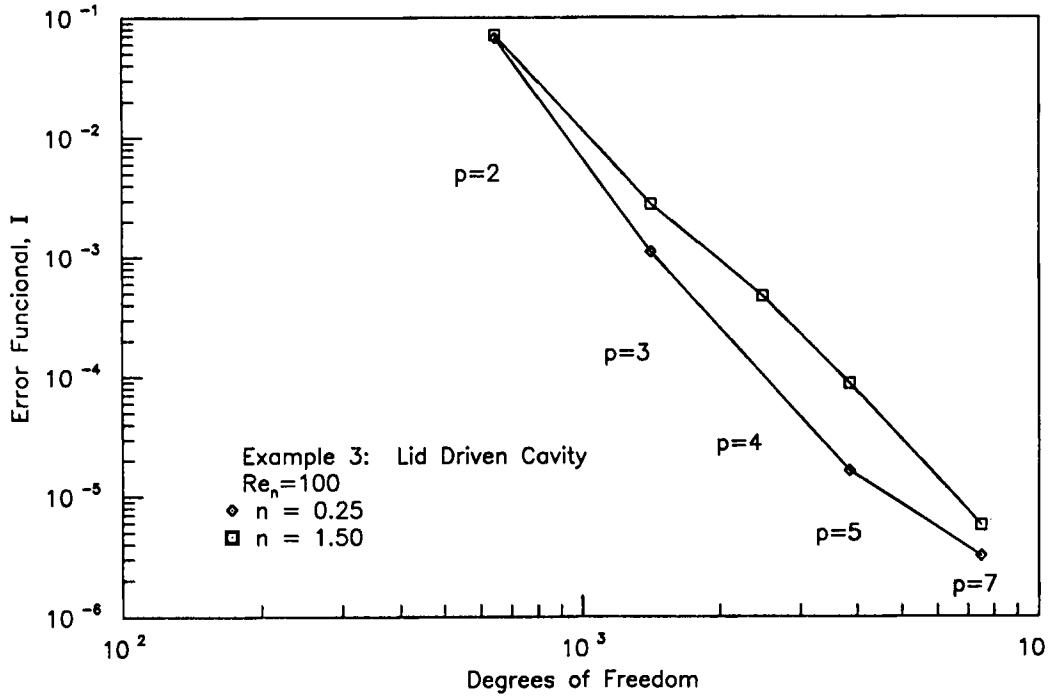

Figure 17. p-Convergence of the error functional I for $n = 0{\cdot}25$ and $1{\cdot}50$ (Example 3)

and

$$T = \frac{Br_n}{\beta^{2n}} \frac{n}{3n+1} \left(\frac{2n+1}{n}\right)^n \left[1 - \left(\frac{y}{\beta}\right)^{(3n+1)/n}\right], \tag{33}$$

where β is the channel half-width. No boundary conditions were specified at the exit.

This 132-element model was arrived at by starting with a coarse model and then systematically refining the mesh based on the error functional I^e for the elements. At each stage the p-convergence of the mesh was examined and refinement was made in the areas containing elements with relatively high values of the element error functional. The solutions obtained using the 132-element mesh were sufficiently accurate when the p-level was increased to four or five. Increasing the number of elements beyond 132 or the p-level above five did not significantly improve the results for any of the wide range of flow conditions examined here. The smallest element length in this mesh was 0·02 for elements located near the corner at the contraction. A maximum of seven iterations were needed for a convergence tolerance of 10^{-4} or less for both $\{g\}$ and I.

The Reynolds number for this problem is defined as $Re_n = \rho_0 u_{avg}^{2-n} h^n / m_0$, where ρ_0 and m_0 are evaluated at the wall temperature and h is the half-width of the contraction (for a Newtonian fluid $n = 1{\cdot}0$ and $m_0 = \mu_0$). The value of Re_n is held constant at 10 in order to concentrate on the effects of the other dimensionless parameters. This particular value for Re_n is chosen to ensure that both convection and diffusion terms are significant. The dimensionless temperature is defined as $T = (\hat{T} - T_0)/(T_{max,c} - T_0)$, where $T_{max,c}$ is the maximum temperature occurring in fully developed channel flow for a Newtonian fluid with-

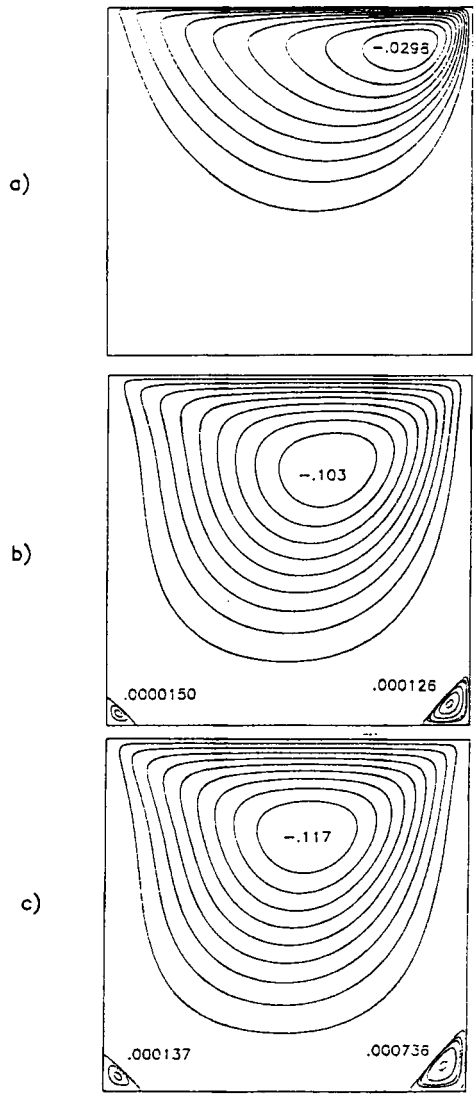

Figure 18. Streamline plots for the driven cavity problem for power-law indices of (a) 0·25, (b) 1·0 and (c) 1·5. The numbers represent the maximum streamline values of the vortex. $Re_n = 100$

out a temperature-dependent viscosity and for $Br = 1{\cdot}0$. The analytical expression for $T_{\max,c}$ is

$$T_{\max,c} = Bru^2_{\max,c}/3. \tag{34}$$

For a unit flow rate in the upper half of the contraction, $u_{\max,c} = 1{\cdot}5$, and with $Br = 1{\cdot}0$, $T_{\max,c} = 0{\cdot}75$. The Brinkman number, which determines the importance of viscous dissipation, is defined as $Br_n = m_0 u_{avg}^{n+1}/k_0 h^{n-1}(T_{\max,c} - T_0)$.

The Peclet number represents the ratio of heat transfer by convection to that by conduction and was defined as $Pe = \rho_0 C_{p_0} u_{avg} h/k_0$. The values of Br_n, Pe_n, n (power-law index) and A (characteristic temperature difference of the fluid, equation (32)) were all varied over wide ranges in order to examine the characteristics of the current formulation.

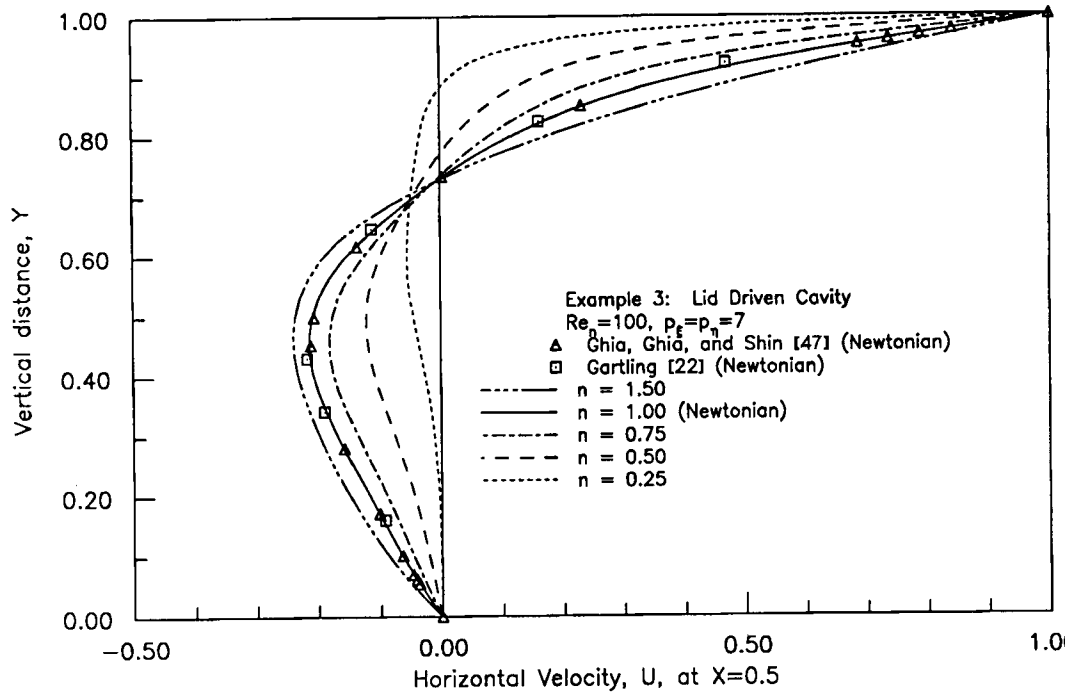

Figure 19. Converged horizontal velocity (u) profiles at $x = 0{\cdot}5$ for various values of the power-law index (Example 3)

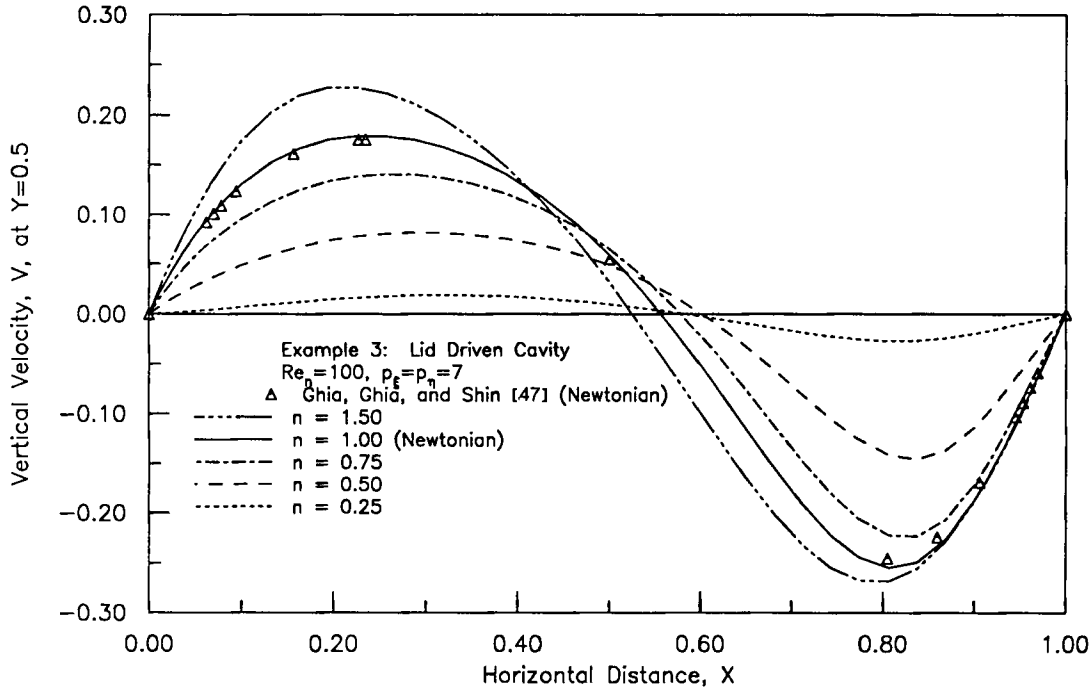

Figure 20. Converged vertical velocity (v) profiles at $y = 0{\cdot}5$ for various values of the power-law index (Example 3)

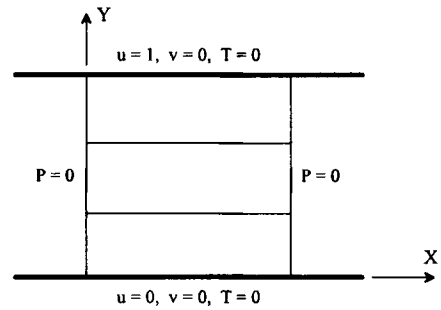

Figure 21. Schematic and finite element model for the Couette shear flow problem (Example 4)

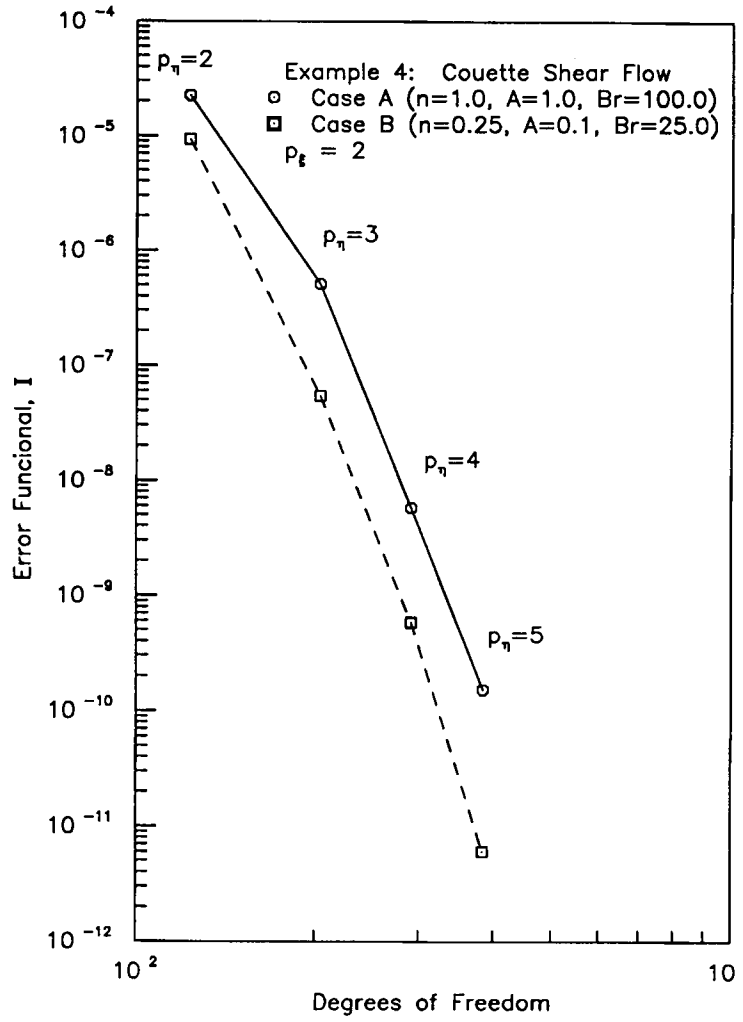

Figure 22. *p*-Convergence of the error functional I for cases A and B (Example 4)

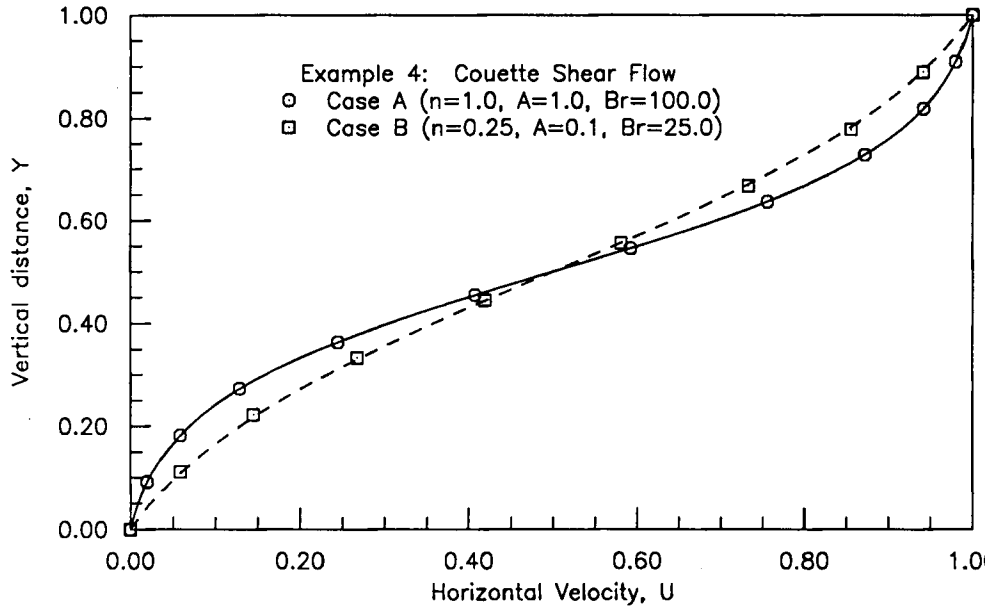

Figure 23. Converged horizontal velocity profiles for cases A and B. Symbols represent the analytical solution (Example 4)

In this study the p-levels in the ξ- and η-directions were increased uniformly for all elements. Figure 26 shows two representative plots of the error functional versus DOF. Case A is for a Newtonian fluid and case B is for a power law fluid, both with a temperature-dependent viscosity (defined by equation (30)). Note the rapid improvement in the error functional with increasing p-level. At a p-level of four or five the solution is essentially converged, with values of the

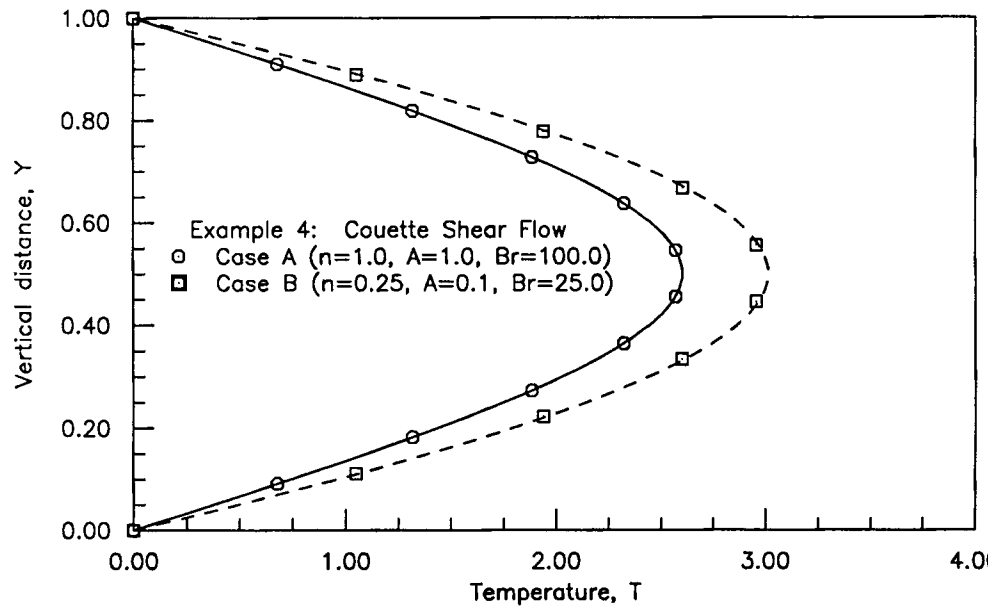

Figure 24. Converged temperature profiles for cases A and B. Symbols represent the analytical solution (Example 4)

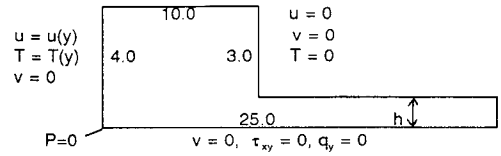

a)

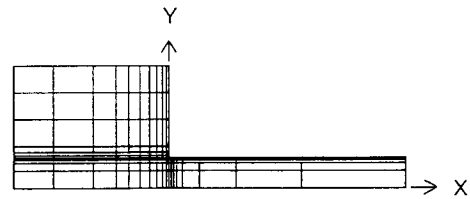

b)

Figure 25. Schematic and finite element model of the 4:1 symmetric sudden contraction: (a) schematic and boundary conditions; (b) graded 132 p-version finite element mesh (Example 5)

error functional of the order of 10^{-4}. Similar p-convergence trends were observed for all other flow conditions examined here.

The solutions obtained for Newtonian fluid flow are described first. Figure 27 is a representative streamline plot (the plots for all Newtonian cases were essentially similar in appearance) showing a region of recirculation in the upper corner. This pattern is very similar to results published by numerous other authors.[32,34,35,38,48] The flow in the inlet region is essentially isothermal (illustrated later) in all cases, so that the value of A had little effect on the velocity field there. Changes in the temperature field with changes in Br, A and Pe are much more significant. Figures 28(a)–28(d) show isotherms for Peclet numbers of 1, 10, 100 and 1000 respectively, while Br and A are held constant. From these isotherms we note the influence of increased heat transfer due to convection (as compared with conduction) on the shape of the contours and the maximum temperature in the flow field. From Figure 28(a) we note that there is a local 'hot spot' on the centreline just below the corner at the contraction. This 'hot spot' has also been observed by Douglas and Roylance[37] and Mitsoulis and Vlachopoulos[38] for low Peclet numbers. This 'hot spot' disappears as Pe increases. It is worth noting that the flow at the exit is fully developed only for $Pe = 1$. For higher Pe the length of the exit region would have to be extended in order to reach the fully developed flow state.

The effect of the temperature-dependent viscosity on the centreline temperature is demonstrated in Figures 29 and 30. These figures show the centreline temperatures for four different Peclet numbers and $A = 0$ and 0·1. The results in Figure 29 are for a Brinkman number $Br = 1$ and those in Figure 30 are for $Br = 10$. These figures show that the differences in centreline temperatures between fluids with a temperature-independent viscosity ($A = 0$) and those with a temperature-dependent viscosity ($A = 0{\cdot}1$) increases when the relative importance of viscous

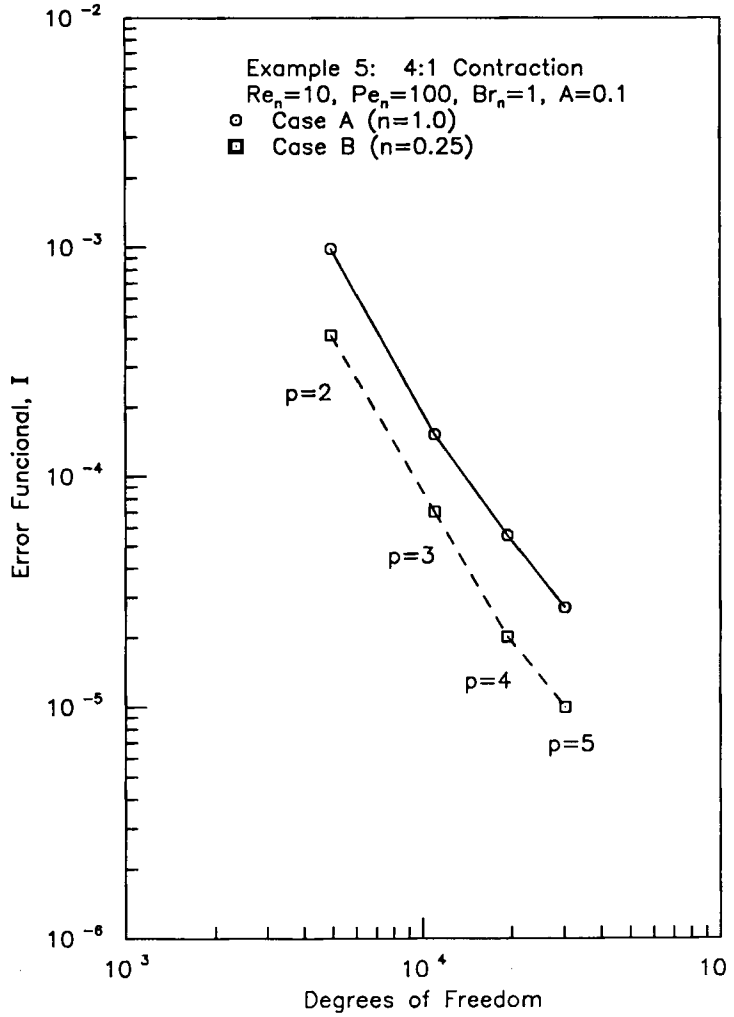

Figure 26. p-Convergence of the error functional I for a Newtonian fluid (case A) and a power-law fluid (case B) (Example 5)

Figure 27. Streamline plot for the flow of a Newtonian fluid in a 4:1 symmetric sudden contraction (Re = 10, Pe = 100, Br = 1, A = 0·1) (Example 5)

dissipation increases. We also note that these curves are smooth and do not contain the spurious oscillations which often result in solutions obtained from Galerkin-based formulations without the use of upwinding.

The results obtained for power-law fluids (shear thinning) are not drastically different from the results for a Newtonian fluid. We have already seen from Figure 26 that the convergence

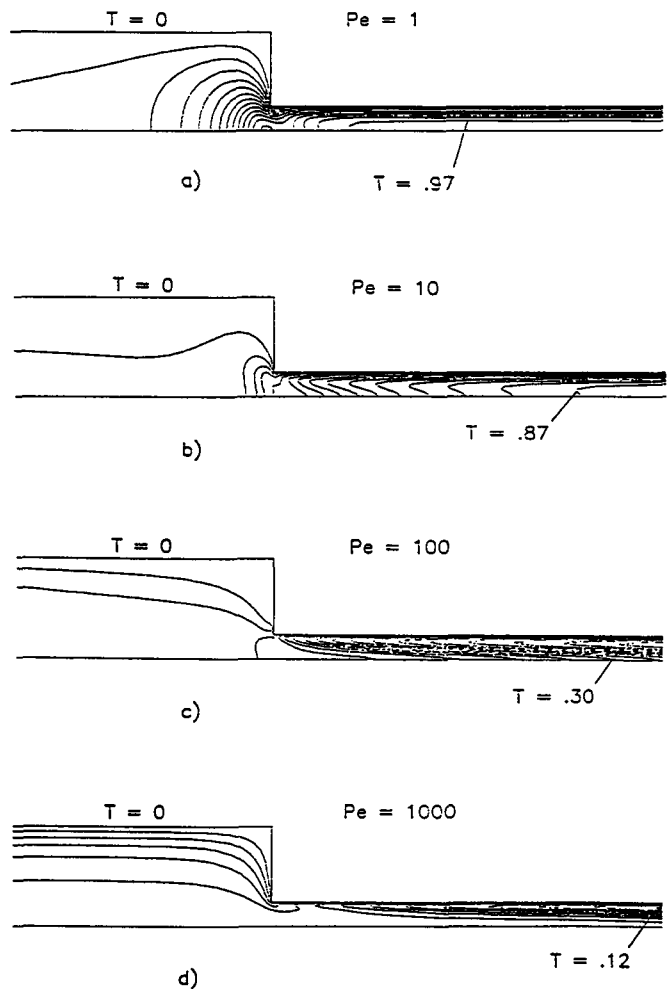

Figure 28. Isotherm plots for the flow of a Newtonian fluid in a 4:1 symmetric sudden contraction: (a) $Pe = 1$; (b) $Pe = 10$; (c) $Pe = 100$; (d) $Pe = 1000$. In all cases $Re = 10$, $Br = 1$ and $A = 0{\cdot}1$ (Example 5)

characteristics of the two fluids are very similar. Figure 31 shows streamline and isotherm plots for a shear-thinning fluid with a power-law index of 0·25. Comparing this streamline pattern with the pattern for a Newtonian fluid given in Figure 27, it can be seen that the two are very similar except that the region of recirculation which is present for the Newtonian fluid is absent for the shear-thinning fluid. This observation has also been reported previously.[31]

CONCLUSIONS

A true (free of approximations and assumptions) *p*-version least squares finite element formulation has been presented for the two-dimensional, incompressible, steady state flow of a power-law fluid under isothermal or non-isothermal conditions. In the development of the least squares error functional, actual non-linear partial differential equations were utilized without linearizing

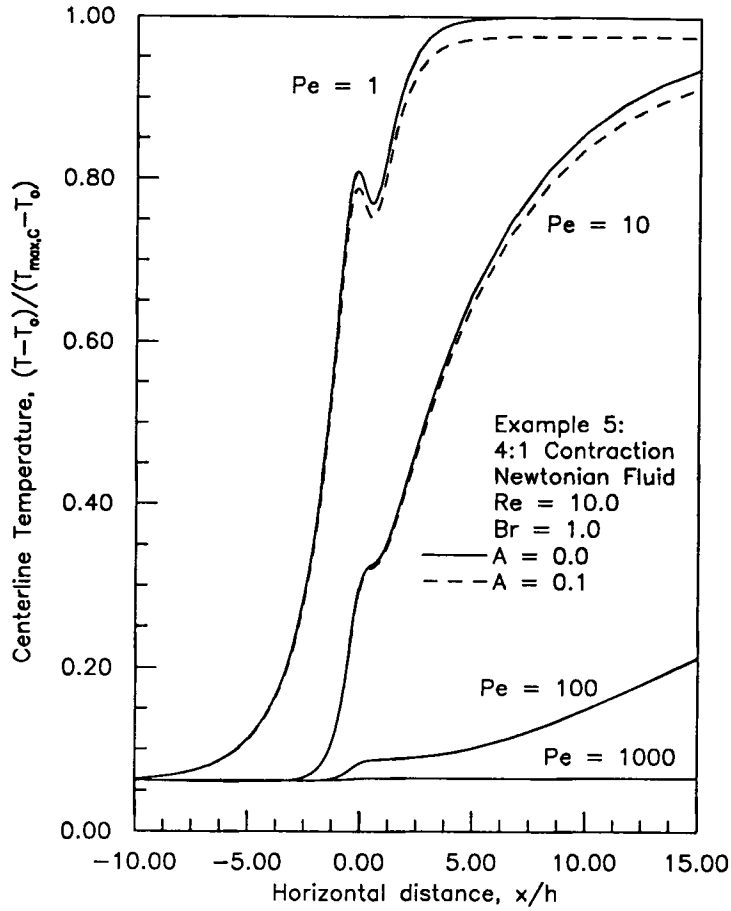

Figure 29. Centreline temperature versus horizontal distance for a Newtonian fluid with $Re = 10$, $Br = 1$ and for four different values of Pe. The solid curves are for $A = 0$ and the dashed curves are for $A = 0{\cdot}1$ (Example 5)

the non-linear terms or introducing any other approximations. Newton's method with a line search was utilized to find the solution which satisfies the conditions resulting from the least squares minimization principle. Five numerical examples are presented for isothermal and non-isothermal conditions. The computed solutions in these examples show excellent agreement with analytical solutions and with solutions reported in the literature for a wide range of power-law indices ($0{\cdot}25 \leqslant n \leqslant 1{\cdot}5$).

The particular choice of the non-dimensional form of the equations of fluid motion was found to be very important with regard to solution accuracy and efficiency of the iterative solution procedure. A generalization can be made that when using non-dimensional equaions in the LSFEF, the non-dimensional form should be chosen such that the relative weight of each equation is not strongly affected by the value of any dimensionless parameter contained in the equations. The results of this work showed that when the Reynolds number appeared in the stress equations (instead of the momentum equations), better p-convergence was attained and the solution procedure required no more than seven iterations for the range of power-law indices reported here.

For the non-isothermal case the viscosity and thermal conductivities were functions of

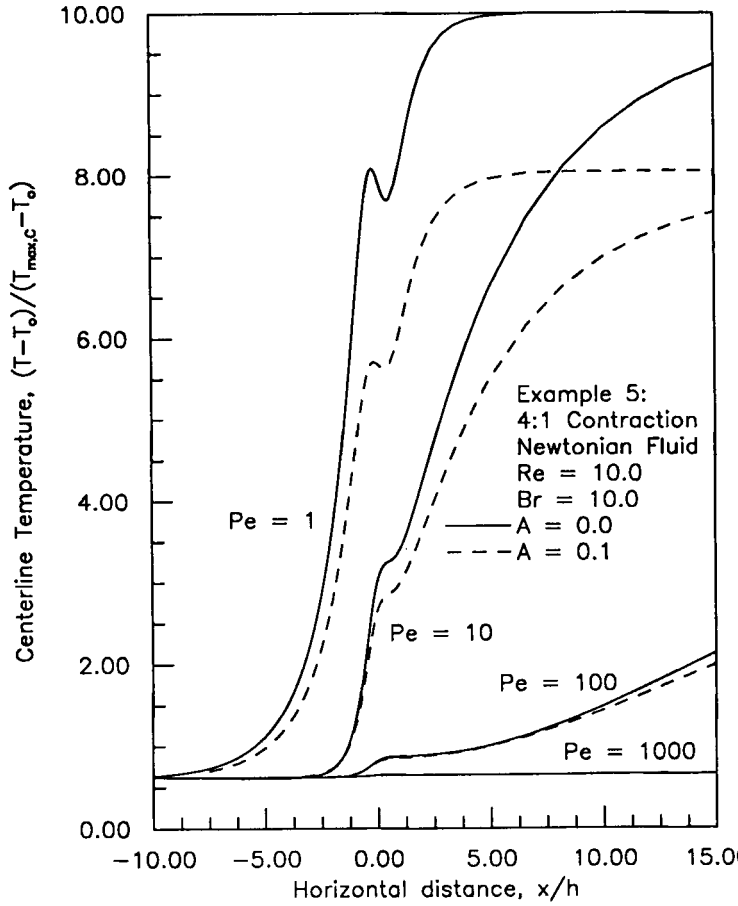

Figure 30. Centreline temperature versus horizontal distance for a Newtonian fluid with $Re = 10$, $Br = 10$ and for four different values of Pe. The solid curves are for $A = 0$ and the dashed curves are for $A = 0{\cdot}1$ (Example 5)

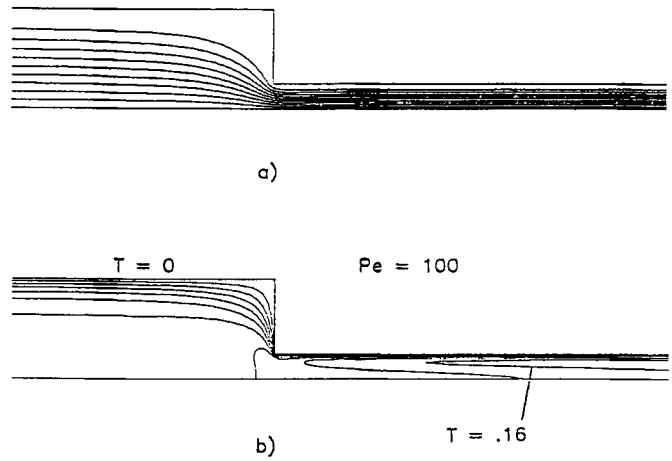

Figure 31. Flow of a power-law fluid ($n = 0{\cdot}25$) in a 4:1 symmetric sudden contraction ($Re = 10$, $Pe = 100$, $Br = 1$, $A = 0{\cdot}1$): (a) streamline plot; (b) isotherm plot (Example 5)

temperature and thus the energy equation was fully coupled with the continuity and momentum equations. The least squares finite element procedure automatically provides a measure of solution error in the form of the error functional. The element error functional values are ideal for adaptive *h*- or *p*-refinements and in fact have been used in obtaining the final graded meshes presented in this paper for the numerical examples. The total error functional for the entire model is a monotonic function of the total degrees of freedom as the *p*-levels are increased for a fixed mesh.

In summary, the *p*-version least squares formulation presented here using the '$2p + 1$ integration rule' produces excellent results for all values of the power-law index in the range $0{\cdot}25 \leq n \leq 1{\cdot}5$, has excellent convergence characteristics and provides a general and accurate numerical simulation tool for two-dimensional, isothermal and non-isothermal, incompressible, steady state, generalized Newtonian fluid flow.

ACKNOWLEDGEMENTS

The computing facilities provided by the Computational Mechanics Laboratory (CML) of the Department of Mechanical Engineering are gratefully acknowledged. The financial support provided to the first author by the Department of Mechanical Engineering through the Carey Fellowship is also acknowledged. The authors wish to thank Dr. P. M. Gresho for many valuable suggestions which have helped in improving the quality of presentation in the paper.

REFERENCES

1. D. Winterscheidt and K. S. Surana, '*p*-Version least squares finite element formulation for two-dimensional, incompressible fluid flow', *Int. j. numer. methods fluids*, in press.
2. T. J. R. Hughes, W. K. Liu and A. Brooks, 'Finite element analysis of incompressible viscous flows by the penalty function formulation', *J. Comput. Phys.*, **30**, 1–60 (1979).
3. A. N. Brooks and T. J. R. Hughes, 'Streamline upwind/Petrov–Galerkin formulations for convection dominated flows with particular emphasis on the incompressible Navier–Stokes equations', *Comput. Methods Appl. Mech. Eng.*, **32**, 199–256 (1982).
4. G. F. Carey and R. Krishnan, 'Continuation techniques for a penalty approximation of the Navier–Stokes equations', *Comput. Methods Appl. Mech. Eng.*, **48**, 265–282 (1985).
5. T. J. R. Hughes, L. P. Franca and M. Balestra, 'A new finite element formulation for computational fluid dynamics: V. Circumventing the Babuska–Brezzi condition: a stable Petrov–Galerkin formulation of the Stokes problem accommodating equal-order interpolations', *Comput. Methods Appl. Mech. Eng.*, **59**, 85–99 (1986).
6. T. J. R. Hughes and L. P. Franca, 'A new finite element formulation for computational fluid dynamics: VII. The Stokes problem with various well-posed boundary conditions: symmetric formulations that converge for all velocity/pressure spaces', *Comput. Methods Appl. Mech. Eng.*, **65**, 85–96 (1987).
7. B. N. Jiang and L. A. Povinelli, 'Least squares finite element method for fluid dynamics', *Comput. Methods Appl. Mech. Eng.*, **81**, 13–37 (1990).
8. M. Becker, *The Principles and Applications of Variational Methods, Research Monograph 27*, Massachusetts Institute of technology Press, Cambridge, MA, 1964.
9. P. P. Lynn and S. K. Arya, 'Use of the least squares criterion in the finite element formulation', *Int. j. numer. methods eng.*, **6**, 75–88 (1973).
10. G. F. Carey and B. N. Jiang, 'Least-squares finite elements for first-order hyperbolic systems', *Int. j. numer. methods eng.*, **26**, 81–93 (1988).
11. G. J. Fix and M. D. Gunzburger, 'On least squares approximations to indefinite problems of the mixed type', *Int. j. numer. methods eng.*, **12**, 453–469 (1978).
12. P. P. Lynn, 'Least squares finite element analysis of laminar boundary layer flows', *Int. j. numer. methods eng.*, **8**, 865–876 (1974).
13. J. F. Polk and P. P. Lynn, 'A least squares finite element approach to unsteady gas dynamics', *Int. j. numer. methods eng.*, **12**, 3–10 (1978).
14. B. N. Jiang and C. L. Chang, 'Least-squares finite elements for the Stokes problem', *Comput. Methods Appl. Mech. Eng.*, **78**, 297–311 (1990).
15. C. A. J. Fletcher, 'A primitive variable finite element formulation for inviscid, compressible flow', *J. Comput. Phys.*, **33**, 301–312 (1979).
16. H. Nguyen and J. Reynen, 'A space–time least-squares finite element scheme for advection–diffusion equations', *Comput. Methods Appl. Mech. Eng.*, **42**, 331–342 (1984).

17. I. Kececioglu and B. Rubinsky, 'A mixed-variable continuously deforming finite element method for parabolic evolution problems. Part II: The coupled problem of phase-change in porous media', *Int. j. numer. methods eng.*, **28**, 2609–2634 (1989).
18. I. Babuska, O. C. Zienkiewicz, J. Gago and E. R. de A. Oliveira, *Accuracy Estimates and Adaptive Refinements in Finite Element Computations*, Wiley, New York, 1986.
19. B. N. Jiang and V. Sonnad, 'Least-squares solution of incompressible Navier–Stokes equations with the *p*-version of finite elements', *NASA Tech. Memo. 105203, ICOMP-91-14* September 1991.
20. D. Winterscheidt and K. S. Surana, '*p*-Version least squares finite element formulation for Burgers' equation', *Int. j. numer. methods eng.*, in press.
21. D. Winterscheidt and K. S. Surana, '*p*-Version least squares finite element formulation for convection–diffusion problems', *Int. j. numer. methods eng.*, **36**, 111–133 (1993).
22. D. K. Gartling, 'Finite element methods for non-Newtonian flows', *Sandia National Laboratories Rep. SAND85-1704*, 1986.
23. G. F. Carey, K. C. Wang and W. D. Joubert, 'Performance of iterative methods for Newtonian and generalized Newtonian flows,', *Int. j. numer. methods fluids*, **9**, 127–150 (1989).
24. O. R. Sorensen and J. Reffstrup, 'Simulation of generalized Newtonian flow using finite element method with an improved iterative procedure', in *Numerical Methods for Non-linear Problems*, Vol. 3, Pineridge, Swansea, 1986.
25. H. H. Dannelongue and P. A. Tanguy, 'An adaptive remeshing technique for non-Newtonian fluid flow', *Int. j. number. methods eng.*, **30**, 1555–1567 (1990).
26. K. C. Wang and G. F. Carey, 'Adaptive grids for coupled viscous flow and transport', *Comput. Methods Appl. Mech. Eng.*, **82**, 365–383 (1990).
27. J. F. Lyness, D. R. J. Own and O. C. Zienkiewicz, 'Finite element analysis of the steady flow of non-Newtonian fluids through parallel sided conduits', in *Finite Element Methods in Flow Problems*, UAH Press, Huntsville, AL, 1974.
28. R. M. Turian and R. B. Bird, 'Viscous heating in the cone-and-plate viscometer—II', *Chem. Eng. Sci.*, **18**, 689–696 (1963).
29. R. M. Turian, 'Viscous heating in the cone-and-plate viscometer—III', *Chem. Eng. Sci.*, **20**, 771–781 (1965).
30. D. V. Boger, *Advances in Transport Processes*, Vol. II, Wiley, New York, 1982.
31. D. V. Boger, 'Viscoelastic flows through contractions', *Ann. Rev. Fluid Mech.*, **19**, 157–182 (1987).
32. E. Mitsoulis and J. Vlachopoulos, 'Effect of Reynolds number in laminar flow through a sudden planar contraction', *AIChEJ.*, **31**, 1736–39 (1985).
33. J. N. Reddy, V. A. Padhye and M. Iga, 'A penalty finite element model for flows of non-Newtonian fluids', in *Numerical Methods in Laminar and Turbulent Flow*, Vol. 5, Part 2, Pineridge, Swansea, 1987.
34. M. J. Crochet, A. R. Davies and K. Walters, *Numerical Simulation of Non-Newtonian Flow*, Elsevier, new York, 1984.
35. D. M. Hawken, P. Townsend and M. F. Webster, 'Numerical simulation of viscous flows in channels with a step', *Comput. Fluids*, **20**, 59–75 (1991).
36. F. Durst, W. F. Schierholz and A. M. Wunderlich, 'Experimental and numerical investigations of plane duct flows with sudden contractions', *Trans. ASME*, **109**, 376–383 (1987).
37. C. Douglas and D. Roylance, *Finite Element Flow Analysis*, North-Holland, New York, 1982.
38. E. Mitsoulis and J. Vlachopoulos, 'Non-isothermal creeping flow through parallel plates and a sudden contraction', *Can. J. Chem. Eng.*, **62**, 832–844 (1984).
39. P. A. Tanguy and A. Fortin, 'A finite element simulation of polymer melt flows', *Adv. Polym. Technol.*, **6**, 501–508 (1986).
40. P. A. Tanguy, M. Fortin and L. Choplin, *Int. j. numer. methods fluids*, **4**, 459–466 (1984).
41. R. B. Bird, W. E. Steward and E. N. Lightfoot, *Transport Phenomena*, Wiley, New York, 1960.
42. R. B. Bird, R. C. Armstrong and O. Hassager, *Dynamics of Polymeric Liquids*, Vol. 1, Wiley, New York, 1987.
43. P. P. Lynn and S. K. Arya, 'Finite elements formulation by the weighted discrete least squares method', *Int. j. numer. methods eng.*, **8**, 71–90 (1974).
44. O. C. Zienkiewicz and D. R. J. Owen, 'Least squares-finite element for elasto-static problems, use of "reduced" integration', *Int. j. numer. methods eng.*, **8**, 341–358 (1974).
45. G. Georgiou, W. Schultz and L. Olson, 'Singular finite elements for the sudden-expansion and die-swell problems', *Int. j. numer. methods fluids*, **10**, 357–372 (1990).
46. G. Schneider and M. Raw, 'Control volume finite-element method for heat transfer and fluid flow using collocated variables—2. Application and validation', *numer. heat Transfer*, **11**, 291–400 (1987).
47. U. Ghia, K. N. Ghia and C. T. Shin, 'High-*Re* solutions for incompressible flow using the Navier–Stokes equations and a multigrid method', *J. Comput. Phys.*, **48**, 387–411 (1982).
48. T. N. Phillips, 'Spectral domain decomposition techniques for viscous incompressible flows', *Comput. Methods Appl. Mech. Eng.*, **80**, 389–395 (1990).